How to cite: *Angew. Chem. Int. Ed.* **2023**, *62*, e202300319
doi.org/10.1002/anie.202300319

Heterogeneous Catalysis

Carbon Deposit Analysis in Catalyst Deactivation, Regeneration, and Rejuvenation

Eelco T. C. Vogt, Donglong Fu, and Bert M. Weckhuysen**

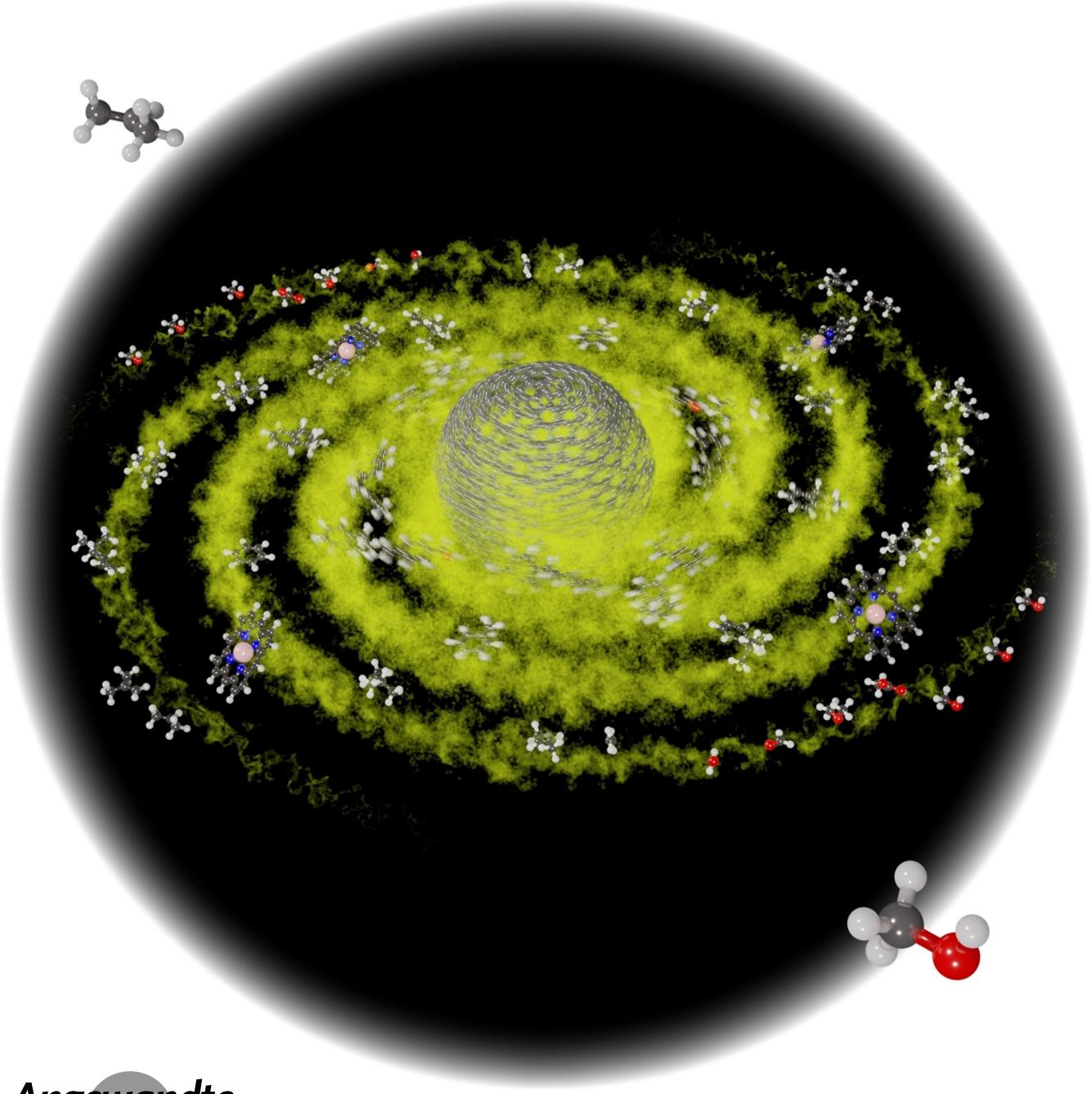

Angewandte International Edition Chemie

Abstract: Hydrocarbon conversion catalysts suffer from deactivation by deposition or formation of carbon deposits. Carbon deposit formation is thermodynamically favored above 350 °C, even in some hydrogen-rich environments. We discuss four basic mechanisms: a carbenium-ion based mechanism taking place on acid sites of zeolites or bifunctional catalysts, a metal-induced formation of soft coke (i.e., oligomers of small olefins) on bifunctional catalysts, a radical-mediated mechanism in higher-temperature processes, and fast-growing carbon filament formation. Catalysts deactivate because carbon deposits block pores at different length scales, or directly block active sites. Some deactivated catalysts can be re-used, others can be regenerated or have to be discarded. Catalyst and process design can mitigate the effects of deactivation. New analytical tools allow for the direct observation (in some cases even under in situ or operando conditions) of the 3D-distribution of coke-type species as a function of catalyst structure and lifetime.

1. Introduction

Heterogeneous catalysts enable the efficient use of scarce raw materials, both renewable (e.g., biomass, polymer waste, and municipal waste) and non-renewable (i.e., crude oil, coal, and natural gas), in a host of hydrocarbon and carbohydrate conversion processes. Although the popular definition of catalysts proposes they are not used in the chemical reaction itself, this does not imply that catalysts have eternal life. Unfortunately, as a matter of fact a variety of chemical and physical processes most often lead to the deactivation of solid catalysts.[1–5] Examples of these processes include loss of function through metal sintering and poisoning, as well as structural degradation processes, such as zeolite dealumination and zeolite framework collapse. Another example of catalyst deactivation is the formation of carbon deposits that block catalyst pores or otherwise prevent access to catalytic sites.[6–9] Catalyst deactivation, therefore, is an important field of both academic and industrial research. A series of international symposia was devoted to the subject for over 30 years,[10–17] and a recent review article addresses the diverse literature on the subject with novel literature analysis tools.[18] In the literature discussed in this review, we observe a gradual move from bulk- and single crystal surface post-mortem analysis on model catalysts to more elaborate spectroscopic techniques that study deactivation mechanisms in complete industrial catalysts, at varying length scales, and as a function of time, either in situ or operando. The fact that catalysts typically deactivate over time makes it hard to define a good moment in the lifetime of the catalyst to determine the activity (or turnover frequency (TOF). In hydroprocessing catalysts, for instance, oxidic precursors are sulfided to form the actual active species. The process creates a hyperactive catalyst that needs to be moderated to "steady state" over a period of several days before the catalyst can handle certain feedstocks. In this "steady state" the catalyst deactivates slowly, typically over a period of several months. It is clear that there is no well-defined point at which the TOF of these catalysts can be determined, and we are actually really testing in the area under the activity curve over time, i.e., the turnover number (TON). Hence, the topic of catalyst deactivation cannot be disconnected from catalyst synthesis and activation processes, and calls for an approach where the entire life of a catalyst is monitored, preferably in an inline manner, thereby allowing to regenerate or rejuvenate catalyst materials when their performance is waning.

This review article specifically focuses on the role of carbon species deposited from the feedstock or formed over time, and ways to mitigate the effects of these carbon species by catalyst design, regeneration or rejuvenation. More specifically, we will treat the process of catalyst deactivation of a number of industrially relevant systems for hydrocarbon conversion processes. We will focus on fluid catalytic cracking (FCC) of oil fractions, catalytic pyrolysis and cracking of biomass and polymer waste, methanol-to-hydrocarbons (MTH), and propane dehydrogenation (PDH), and will briefly discuss hydroprocessing (HPC), Fischer–Tropsch synthesis (FTS), solid acid alkylation, as well as methane dehydroaromatization (MDA). These chemical conversion processes are selected because they represent important hydrocarbon and carbohydrate conversion processes with different mechanisms (i.e., cracking versus C–C coupling, and acid catalysis versus metal catalysis) and hydrogen partial pressures (cracking vs. hydroprocessing), operating under a range of working conditions. Catalysts in these processes range from zeolites (usually shaped with binders), to supported metals and metal compounds, as well as bifunctional catalysts combining zeolites/solid acids and metal functions. Mitigation of the effects of coke deposits depends very much on the role of the solid catalyst in the coke formation or deposition mechanism. Catalyst design, both at molecular level and meso- or macro-level, as well as process design (e.g., in situ-regeneration) can assist in making the solid catalyst and related chemical conversion processes more stable towards deactivation by coke deposition.

[*] Prof. Dr. E. T. C. Vogt, Dr. D. Fu, Prof. Dr. B. M. Weckhuysen
Inorganic Chemistry and Catalysis group, Institute for Sustainable and Circular Chemistry and Debye Institute for Nanomaterials Science, Utrecht University
Universiteitsweg 99, 3584 GC Utrecht (The Netherlands)
E-mail: e.t.c.vogt@uu.nl
b.m.weckhuysen@uu.nl

Dr. D. Fu
Present Address: California Institute of Technology, Department of Chemical Engineering
1200 East California Boulevard, Pasadena, CA 91125 (USA)

2. Formation Processes of Carbon Deposits

2.1. Coke Formation Mechanisms

It is important to mention here that "coke" is such a broad term as to be almost useless for the catalyst practitioner. We will follow an adapted version of the definition for coke as formulated by Karge:[19] *Coke consists of carbonaceous species, which have higher average carbon numbers and are hydrogen-deficient compared to the average reactant molecule(s) in the feedstock.* As observed by Olsbye et al.,[20] these species will have a lower vapor pressure, and are more bulky than the reactants, and will thus stick to the catalyst surface or in zeolite pores. Coke can be amorphous carbon, high molecular weight polycyclic hydrocarbons, mixtures of aromatic hydrocarbons, methylbenzenes, branched long-chain aliphatics, or sometimes phenolic materials, but smaller and more aliphatic structures can also be considered, e.g., in the case of propane dehydrogenation or lower olefin alkylation. Coke species, especially when deposited from the hydrocarbon feedstock, can in principle also contain heteroatoms,[21,22] but we will not discuss these in detail here. The carbon species are generally formed via a dehydrogenation or hydrogen transfer process in which hydrogen is continuously extracted from the deposited and depositing products that cannot then be moved continuously from the system. However, the exact coke formation process appears to vary across different reaction types.[23,24]

2.1.1. Coke formation in carbon-carbon bond breaking over acid catalysis

We will now discuss the fluid catalytic cracking (FCC) process as exemplary of a carbon-carbon bond breaking acid catalyzed process. In FCC, a relatively heavy hydrocarbon feedstock, typically vacuum gas oil (VGO) or Resid, is cracked at around 540 °C. The catalyst comprises a solid acid zeolite, combined with alumina- or silica-based binder and matrix, as well as clay. Special functions may be introduced for instance for trapping poisoning metals. The FCC process is thus targeting C–C bond breakage and the creation of smaller molecule fractions, typically gasoline range hydrocarbons or lower olefins. During the cracking step a small part of the feedstock is converted into coke. After separating the deactivated catalyst material from the products, the

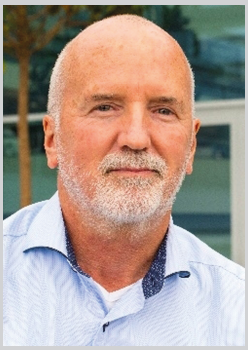

Eelco Vogt obtained his Ph.D. in Inorganic Chemistry and Catalysis in 1988 from Utrecht University (the Netherlands) under the supervision of professor Geus. He has worked for Albemarle Catalysts Company BV (previously Akzo Nobel Catalysts) for over 30 years, working on fluid catalytic cracking, hydroprocessing, hydrocracking, biomass conversion and various other catalytic processes, and was Albemarle's Global Director for Catalyst R&D from 2006 through 2009. He left Albemarle in 2020. Since 2014, he is a professor by special appointment at Utrecht University holding a chair in catalysis of refinery processes, and since 2020 he is a full professor at Utrecht University. He is the former chairman of VIRAN, the Industrial Advisory Board to the Netherlands Research Institute on Catalysis (NIOK), and of the program council Chemical Conversion, Process Technology and Synthesis for the Dutch Topsector Chemistry (ChemistryNL). He is scientific director of the Utrecht University Institute for Sustainable and Circular Chemistry.

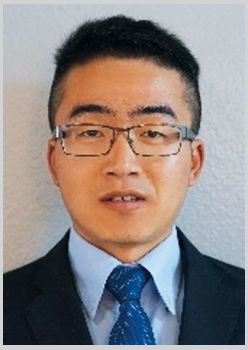

Donglong Fu obtained his Ph.D. in Inorganic Chemistry and Catalysis in 2020 from Utrecht University (the Netherlands) under the supervision of professor Bert Weckhuysen. His Ph.D. thesis focused on development of zeolite films and membranes for sustainable catalysis. Since 2020, he joined the group of professor Mark Davis at California Institute of Technology as a postdoctoral scholar. His research interests are developing in situ and operando spectroscopic techniques for the study of catalysis and sorption under working conditions, as well as microporous materials for carbon capture and conversion.

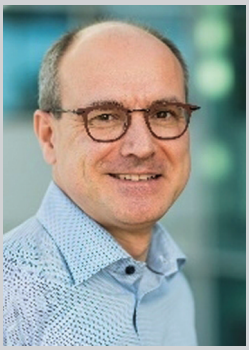

Bert M. Weckhuysen obtained his Ph.D. in Surface Chemistry and Catalysis in 1995 from Leuven University (Belgium) under the supervision of professor Schoonheydt. He conducted two postdoctoral stays in the USA; in the groups of professor Wachs at Lehigh University and of professor Lunsford at Texas A&M University. In 2000, he became full professor at Utrecht University, where he has worked since then on the development and use of different spectroscopy and microscopy methods to investigate catalytic solids under reaction conditions. He has been focusing on connecting nano- and microscale events to the macroworld of catalyst activity, selectivity and stability. His work has been recognized by many research awards, including the Paul Emmett Award in Fundamental Catalysis from the North American Catalysis Society, the International Catalysis Award from the International Association of Catalysis Societies, the John Bourke Award from the Royal Society of Chemistry, the Spinoza Award, the Robert Anderson Award from the Canadian Catalysis Society the Kozo Tanabe Prize in Acid-Base Catalysis and the Chemistry Europe Award. He is an elected member of the KNAW, KVAB and Academia Europaea; and is currently President of the European Federation of Catalysis Societies (EFCATS).

catalyst is regenerated by burning off (most of) the coke deposits at around 700 °C (in the regenerator reactor) and reintroduced in the cracking section (in the riser reactor). Catalysts typically run through thousands of cracking-regeneration cycles during their lifetime (as an indication, an average cracking/regeneration cycle would last about ten minutes). Part of the energy generated by burning off the coke is required to run the endothermic cracking process; the remainder is mostly used to heat the feedstock and accommodate other heat requirements of the process. As we shall see below, the formation of coke is unavoidable thermodynamically, but at the same time it is an energetic requirement for the process: FCC could not run without coke formation.[25]

The formation of coke as a result of catalytic action is very fast,[26,27] and can start from relatively small molecules (i.e., C_3, and C_4), by alkylation, isomerization, ring closure, and dehydrogenation, for instance following the reaction Scheme proposed by Guisnet and Magnoux[28] (Figure 1).

Although one might rightly expect cracking to prevail at FCC conditions, as we will describe in more detail below, the formation of (multiring-)aromatic molecules from smaller building blocks is thermodynamically favored at increased reaction temperatures.[29] Specifically for the coke formation process, as depicted in Figure 1, the endothermic reaction from isobutene and propane to form toluene is thermodynamically favored above ≈350 °C, and the onward reaction to naphthalene is favored above ≈410 °C. In a previous review on the FCC process, we have illustrated with 2D-GC analysis how a predominantly paraffinic feedstock is indeed converted to a product rich in (poly-) aromatic molecules.[25] We should note that the small molecules suggested as the starting point of the coke formation process are secondary products that are formed form cracking gasoline range olefins, which are proposed as the first intermediate products by Guisnet and Magnoux. We may therefore suggest that their conversion to isobutene and propylene would not be required to initiate the formation of coke.

2.1.2. Coke formation in pyrolysis and cracking of biomass and polymer waste

Biomass and polymer waste have been proposed as suitable candidates to replace fossil fuels as raw materials for the manufacturing of transportation fuels and chemicals. Although the process choices may seem similar to cracking fossil fuels, there are some important differences. Compared to catalytic cracking, which typically converts VGO molecules in the C_{30}–C_{40}-range, the challenge lies in the observation that biomass and polymers usually share a polymeric nature (i.e., the molecular weight is much higher, which affects the vaporization, but also the molecules are more chain-like, which complicates molecular diffusion in the pores of the solid catalyst). In addition, the concentration of heteroatoms (e.g., O, N, S, for biomass and also Cl for e.g., PVC, and N and O in e.g., Nylon) is much higher.

The most common conversion processes for biomass and plastic waste rely on pyrolysis. The formation of coke is increased at elevated temperature and pressure. The addition of H_2 (hydrocracking) is an obvious measure to lower coke formation in plastics recycling, but also the

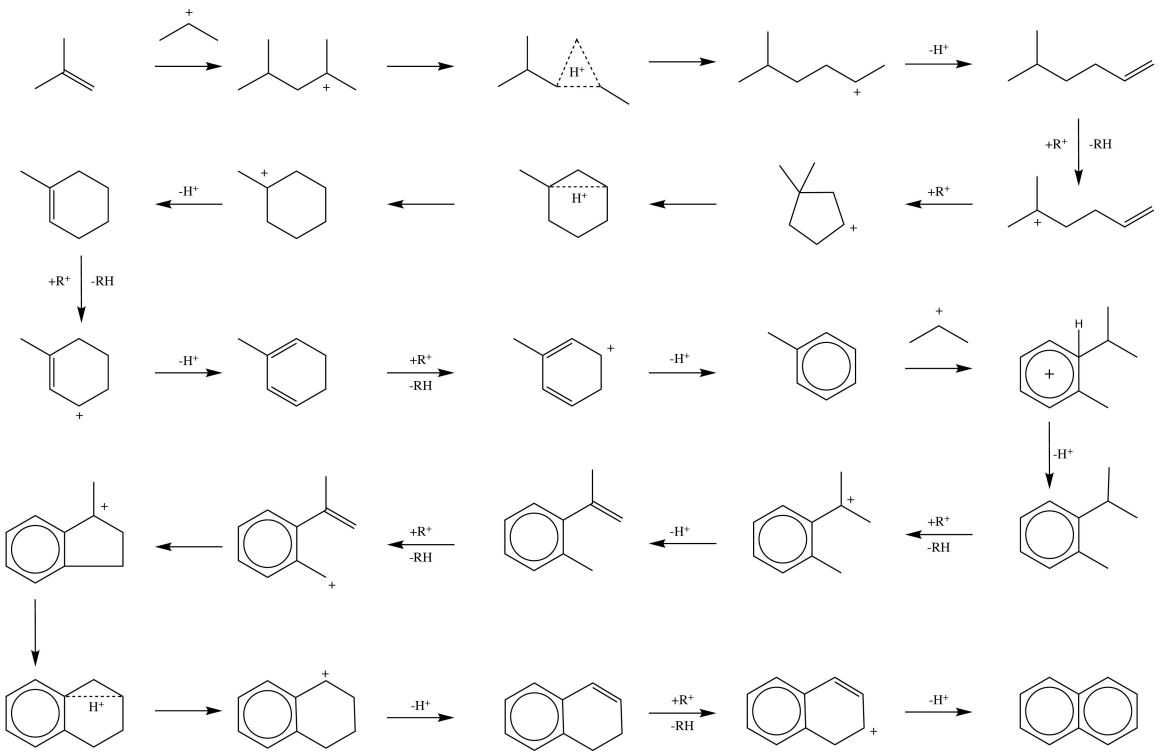

Figure 1. Coke formation mechanism in the fluid catalytic cracking (FCC) process, as proposed by Guisnet and Magnoux. Based on Ref. [15].

addition of CO_2 reduces the formation of tar in the pyrolysis of PVC.[30] Vollmer et al. review the pyrolysis of various plastic waste streams, and conclude that an increase in complexity (number of functional groups and heteroatoms in the backbone) of the polymer increases the selectivity to the monomers, whereas in the pyrolysis of e.g. HDPE, a distribution is observed that looks similar in nature to FCC (olefins and BTX products, i.e. coke precursors).[30] As we explained above, in a previous review on the FCC process, we illustrated with 2D-GC analysis how a predominantly paraffinic feedstock is converted to a (lower average molecular mass) product rich in (poly-)aromatic molecules.[25] This explains the findings of Vollmer et al.,[30] and implies that the selectivity to monomers for a thermocatalytic cracking process for polymers will always be limited. In a subsequent paper, the authors demonstrate that equilibrium FCC catalysts actually outperform fresh FCC catalysts, for instance because of lower coke production.[31]

The conversion of biomass and agricultural waste to commercially interesting chemical intermediates (the so-called platform chemicals) or transportation fuels has been studied in great detail over the past two decades. Biomass can comprise starches and sugars, triglycerides and fatty acids, and finally lignocellulose. The conversion of these different classes requires different processes.[32] A simple option[33,34] is to add biomass (and possible polyolefin plastic waste)[35] as a feedstock component to the conventional refinery conversion processes, like FCC. Starting from fatty acids (from frying fat to palm oil), the conversion to biofuels is also possible. This was developed in a number of different generations, yielding fatty acid methyl esters (FAME) or deoxygenated fatty acids. The deoxygenation products typically need hydro-isomerization conversion processes, which implies that both processes are performed under high-pressure hydrogen (20–80 bar), and coke-production will be limited, as for convectional hydroprocessing. The challenge in converting lignocellulose and sugars/starches is to maintain as much of the chemical functionalities,[36,37] although a number of the processes described seem to focus on fuels.[34,38] Solvolysis and pyrolysis appear to be the processes of choice for the depolymerization of starch- and lignocellulose-based feedstocks. The most important process for the conversion of these carbohydrates is the removal of oxygen, which implies that the production of considerable amounts of CO_2 and H_2O will have to be taken into account in the process design.[39]

It appears from the above observations that the loss of carbon atom efficiency due to coke formation in the conversion of plastic waste and biomass is most relevant for the catalytic pyrolysis and cracking processes. Wang and Gupta[35] described the co-pyrolysis of plastic waste (e.g., PET, HDPE, LDPE, PVC, PP, and PS) and biomass. Most of the plastics when co-pyrolyzed over zeolites (mostly over zeolite ZSM-5) produce "aromatic compounds" as the main product, and char and coke yields can be as high as 20 %, and the presence of PVC in the mixture appears to increase the yield of solid residues. There does not seem to be a lot of information on the exact nature of the coke deposits formed.

2.1.3. Coke formation in the dehydroaromatization of methane

Although the methane dehydroaromatization (MDA) process is performed with a bifunctional catalyst (e.g., transition metals like Mo W or Fe on zeolite HZSM-5[40,41]), the main deactivation mechanism seems to be the formation of a carbonaceous deposit on the outside of the zeolite particles, blocking the access to the zeolite interior, where the acid functionalities are positioned. The MDA reaction relies on Mo-, W-, or Fe-species to convert the methane into ethylene most probably via an acetylene-like intermediate, and subsequent aromatization of ethylene over the zeolite-based Brønsted acid sites.[42] While the removal of surface BAS by sylilation of the outer surface reduces but does not eliminate the deactivation of the catalyst,[43] coke formation inside the zeolite crystals should also be considered, and the distribution of the metal sites, actually in the form of (a combination of) metal carbides or metal (oxide) carbides, and Brønsted sites is an important design parameter.[40,41] Weckhuysen et al. analyzed the nature of the surface carbon species formed over Mo-HZSM-5 catalysts with X-ray photoelectron spectroscopy (XPS), and concluded three different species could be observed, namely adventitious or graphitic-like deposits, carbidic-like deposits, and hydrogen-poor sp-type deposits. The authors conclude that the sp-hybridized species is predominantly found on the surface of the solid catalysts, and is thus responsible for the main deactivation mechanism.[44] The coke formation mechanisms thus seem to be similar to those in catalytic cracking. Kosinov et al. recently observed that the MDA reaction produces about twice as many product molecules as there are reactant molecule, so thermodynamically we should expect lower deactivation rates at increasing pressure, which is indeed observed when performing the reaction at 15 bar.[45]

2.1.4. Coke formation in the carbon-carbon bond formation over acid catalysis

We will now discuss the methanal-to-hydrocarbons (MTH) process as exemplary of a carbon-carbon bond forming acid catalyzed process. The catalytically active sites are Brønsted acid sites in zeolitic or zeotype catalyst, typically possessing the framework structure MFI (HZSM-5) or CHA (HSAPO-34 or HSSZ-13) at 350–550 °C. This process targets the formation of C–C bonds and the creation of larger molecules from the C_1 molecule. A recent overview by Yarulina et al.[46] describes the transition in literature, based on recent direct observation of the reaction intermediates, from an impurities-based mechanism to a direct mechanism in which the carbonylation of methanol plays a central role in the formation of the first C–C bond. Generally, the direct mechanism and hydrocarbon pool (HCP) mechanism were observed in the initial stage and autocatalysis stage of the MTH process, respectively.[47–51] The first C–C bond formation in the direct mechanism involves the Koch carbonylation and carbene process from surface methoxy species (SMS) to form surface acetate species (see Figure 2).

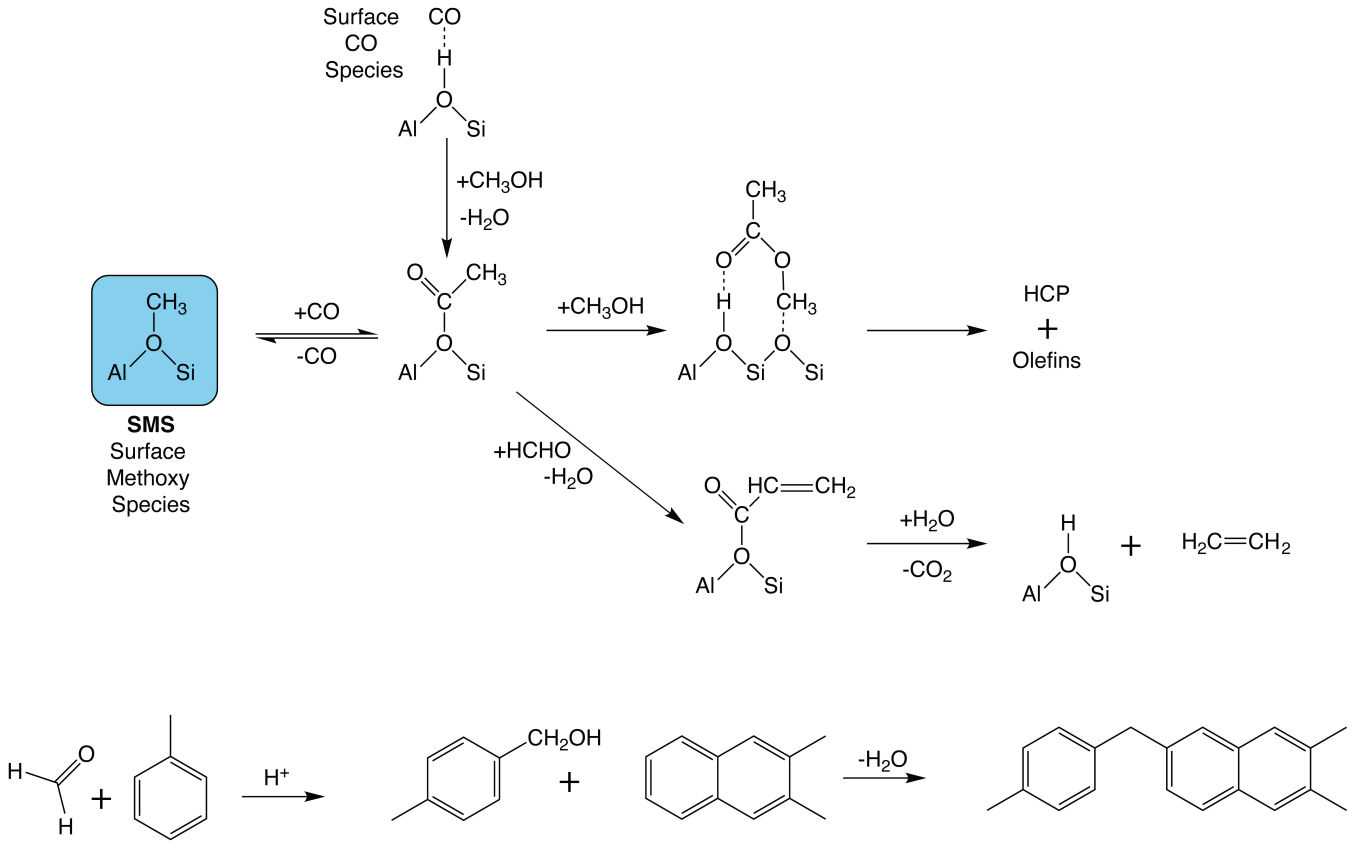

Figure 2. Reaction and coke formation mechanism during the methanol-to-hydrocarbons (MTH) process.[48,49,52–56] Original work. Copyright © 2023 the authors.

These surface acetate species further convert to smaller olefins through ketene intermediates, which initiate the autocatalysis stage with both the dual cycle and HCP mechanism, parallelly working for the production of ethylene and propylene. In an alternative route proposed in the literature, the initial C–C bond formation results from methoxylation of surface CO. This leads to the formation of small ketene ($R_2C{=}C{=}O$) intermediates, which cannot be directly observed but can be inferred from the observation of surface acetate species.[57] Based on theoretical arguments, Pleßow and Stüdt propose that the ketenes undergo successive methylation(s) and decarbonylation to form olefins during the MTH process over zeolites[58] (one of the decarbonylation steps provides the CO for the initiation step).

The formation of aromatic species is crucial to the mechanism of the MTH process,[59] which produces most of the ethylene. However, it can also grow into larger aromatic species leading to catalyst deactivation by either blocking the internal zeolite channels or covering the external surface of the zeolite crystals. Therefore, it is critical to discuss the generation of aromatics in the MTH process:

1) *Small olefinic species to aromatics.* The small olefins formed from ketenes discussed above can transfer into aromatics through several reactions, such as oligomerization, cyclization, hydrogen transfer, and alkylation. The bigger olefinic and aromatic species are key compounds of the alkene and arene cycle of the dual-cycle/HCP mechanism, responsible for the autocatalytic part of the reaction.[48,52] At the same time, paraffins are reproduced by hydride transfer to carbenium ions.[60]
2) *Formaldehyde (HCHO) mediated formation of aromatics.* Generation of formaldehyde under MTH conditions occurs via several pathways, including hydride transfer between two methanol molecules,[53] thermal or reactor-wall catalyzed decomposition of methanol[49] and hydrogen transfer from methanol to alkenes on Lewis acid sites (LAS).[54] Formaldehyde then reacts with surface acetyl groups (from CO and surface methoxy groups as above) to form acrylic acid and larger molecules. Alkenes are subsequently formed by decarboxylation of these carboxylic acids. Formaldehyde is also reactive in the polymerization of the aromatics, e.g., diphenylmethane.[55] The Lercher group showed that formaldehyde can promote the formation of H-poor byproducts, i.e., dienes, aromatics and coke, by reacting with olefins via the Prins reaction.[56] Once the carbon deposits are formed at the external zeolite crystal surface, the external coke can continue to grow even non-catalytically via the thermal reaction with methylated benzene species.[52]

This latter reaction is a fundamentally different reaction mechanism for coke formation/growth, that does not neces-

sarily require catalytic action to proceed once the reactive methylated benzene species are formed catalytically. As such, it is very likely also relevant as a coke formation/growth mechanism in any high-temperature process, such as FCC or (specifically) thermal cracking, but also biomass or plastic waste pyrolysis.[61] Van Speybroeck et al.[62] described the five elementary reversible steps for the gradual reaction of benzene to naphthalene based on a network developed by Wauters and Marin:[63] 1) Hydrogen abstraction from the coke surface by gas-phase radicals, 2) substitution at the coke surface, 3) addition of surface radicals to gas-phase olefins forming gas phase radicals, 4) cyclization, and 5) addition of gas phase radical to surface double bonds (see Figure 3). The resulting reaction networks quickly become very complex.

These complexities generate the debate between the role of surface coke formation and intra-pore blockage. It has been illustrated that intra-pore blockage is predominated for zeolite HZSM-5 deactivation. This can be supported by the observations that short diffusion pathways can reduce deactivation of the zeolite HZSM-5 catalysts. Some examples of this are the long lifetimes of hierarchical zeolites with mesopores acting as highways, and zeolite nanosheets with a unit cell thickness.[64–67] However, a series of studies has demonstrated that surface/external coke formation dictates the deactivation of zeolite ZSM-5.[68–71] The deactivation mechanism of HSAPO-34 catalyst is also not unambiguously understood.[20] Unlike zeolite HZSM-5 catalysts, transient experiments of $^{13}C/^{12}C$ over SAPO-34 suggested that deactivation was initiated by the formation of branched alkanes and alkenes that were trapped in the catalyst cavities, rather than polycyclic aromatics, thereby hindering diffusion and leading to deactivation.[72] This may be caused by the different topologies of the two zeolite materials, HZSM-5 has the MFI framework consisting of medium size 10-membered ring (MR) channels with intersections, while HSAPO-34 is a small pore CHA zeotype material with relatively large cages and 8-MR windows. But a study with the combination of operando UV/Vis and IR spectroscopy coupled with on-line mass spectrometry (MS) measurements concluded that the formation of alkene and polyaromatic species is competitive, suggesting the polyaromatics as being the deactivating species.[73]

2.1.5. Coke formation in hydrotreating processes

Hydroprocessing (HPC), next to FCC, is one of the largest industrial catalytic processes. The catalysts are typically Co- or Ni promoted Mo- or W- sulfides supported on alumina. However, coke formation in HPC has not been studied in as much detail as FCC, likely because catalyst deactivation proceeds much slower due to the presence of a high partial pressure of hydrogen. Nevertheless, quite some studies can be found.[74–84] Maity et al.[75] conclude that mild acid sites on a silica-alumina support can cause the formation of species that differ from those observed on Al_2O_3, Al_2O_3/TiO_2, or carbon supports. These species also form more rapidly. Prajapati et al.[76] ascribe a major role to species in the feed, since aromaticity in the feed correlates to carbon deposition, and the absence of asphaltenes in deasphalted oils results in limited to no coke formation. Richardson et al.[81] studied the effect of pressure, catalyst age and feed composition, and study solid catalysts with large amounts of coke deposits, which makes analysis more feasible. The authors report that in the early stages, metal(-sulfide) sites can

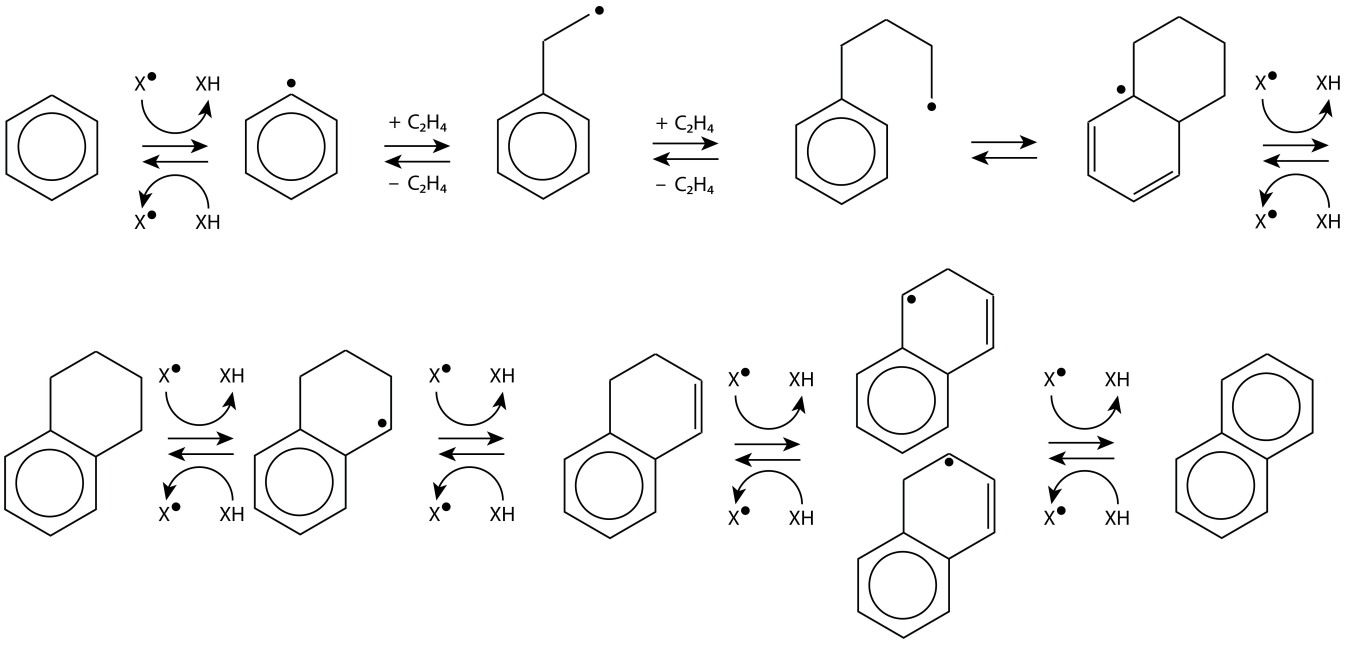

Figure 3. Coke formation reaction from radical mechanism as illustrated by the reaction from benzene to naphthalene. Adapted and generalized with permission from Ref. [62].

hydrogenate coke precursors, but in the later stages these sites are blocked, and pore blocking by growing coke species starts to become significant. This seems to be in agreement with older work.[78–80] For example, Rana et al.[77] used ^{13}C nuclear magnetic resonance (NMR) to analyse the coke on HPC catalysts, but reported only broad features in the aromatic region of the NMR spectrum. Fonseca et al.[74] studied HPC catalysts with coke deposits using ^{13}C NMR, and reported far better resolution in the aromatics region, which allowed them to identify a range of extended aromatic ring structures. Also in this study, the coke load on the HPC catalysts was relatively high (up to 41 wt %).

2.1.6. Coke formation in light alkane dehydrogenation processes

Dehydrogenation of light alkanes, such as propane, is a high temperature process (575–650 °C) mainly conducted over Cr_2O_3/Al_2O_3 (e.g., Catofin® process, Lummus/Chicago Bridge & Iron Company) or Pt-Sn/Al_2O_3 (e.g., Oleflex™ process, UOP/Honeywell) catalyst materials. Sattler et al.[85,86] studied the process with a pilot-scale unit with integrated operando UV/Vis and Raman spectroscopy setup, The authors observed faster coke formation at the bottom of the catalyst bed in the early stages of the reaction, which correlated with a higher bed temperature at the bottom of the catalyst bed.[86] On Pt/Sn-based catalyst materials, Wang et al. report the formation of largely aliphatic coke (i.e., 2/3 of the species), with the remainder aromatic and pre-graphitic coke deposits, mostly on or near the noble metal particle. With diffuse reflectance infrared Fourier transform (DRIFT) spectroscopy they observed the conversion of aliphatic coke deposits to aromatic coke deposits. The authors also note that there is an active role for propene in this deactivation mechanism. However, as Li et al. noted,[87] there is an additional coke formation mechanism that takes place on the metal nanoparticles without a role for acid sites of the support material, probably based on simple propylene oligomerization steps[88] (see Figure 4). The formation of coke precursors on the metal leads to soft coke (i.e., oligomers of small olefins), migration of the dehydrogenated coke precursors to the (acid sites on the) support and subsequent reaction with propylene leads to the formation of hard coke on the acid sites, through a series of chemical reactions not unlike those depicted in Figure 1. It thus appears that the catalytic formation of hard, aromatic-like coke deposits follows a similar route in the FCC, MTH, and PDH processes, with the intermediate molecules entering the mechanism sequence at different steps depending on the application.

It should be noted to the reader that we have thus far described three basic mechanisms for coke formation: a carbenium ion-based reaction sequence taking place on the acid sites of zeolites or an acid surface of bifunctional catalysts (i.e., FCC, MTH, and PDH), a metal-induced formation of soft coke on bifunctional catalysts (although this mechanism is not very much detailed in the literature, and may require the first mechanism to be fully developed in the near future), and finally a radical-mediated mechanism, which is mainly observed in higher-temperature chemical conversion processes (described above for MTH, but also relevant for thermal cracking in FCC).

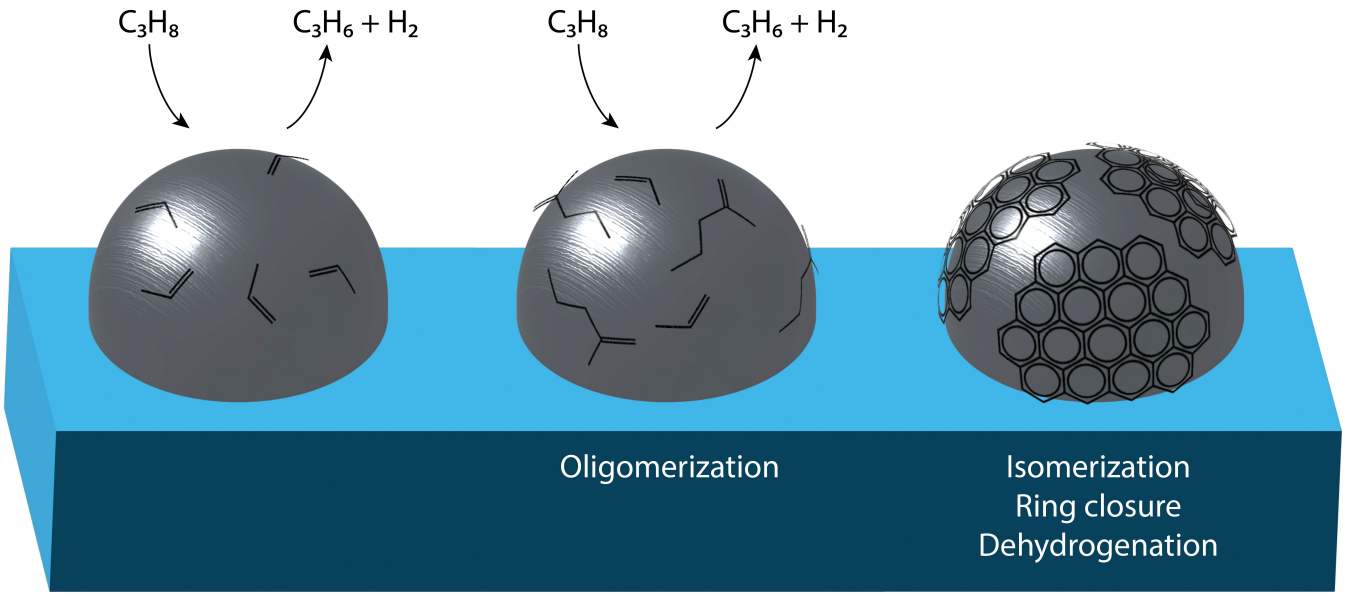

Figure 4. Coke formation in metal-catalysed hydrogenation/dehydrogenation processes involving small olefins, such as propane dehydrogenation (PDH), progressing from left to right. Literature provides only very general descriptions of the steps required. Modified image based on Ref. [89], used with permission.

2.1.7. Coke formation during metal-catalyzed carbon-carbon bond formation processes

The Fischer–Tropsch synthesis process (FTS) is prototypical example of a metal catalyzed carbon-carbon bond formation process. Interestingly, this leads to a fourth mechanism for the formation of coke species, i.e. the formation of carbon filaments. In the FTS process the formation of carbon-carbon bonds is the intended process, and the overall goal is to control the number of carbon atoms in the reaction product.

The initial step in the FTS process is the adsorption of CO on the catalyst surface. This step can be either dissociative or non-dissociative, leading to different products. Hydrogen is adsorbed at the catalyst surface and directly dissociates. The hydrogen atoms may assist in the dissociation of CO, to form H_2O and various $C_1O_yH_z$ monomer-intermediates, such as CH_3 (methyl), CH_2 (methylene), CH (methylidyne), CHO (formyl), HCOH (hydroxycarbene), CH_2OH (hydroxymethyl), and COH (hydroxymethylidine) species. Dissociation of the CO without the requirement of hydrogen species is proposed to produce mobile (sub-)surface oxide and carbide species, especially on iron-based FTS catalysts.[90–93] Various chain growth mechanisms have been proposed, mostly using methylene (CH_2) and methylidine as the reacting monomers. However, since alcohols are also observed in the FTS products, we must assume at least some of the $C_1H_yO_z$ species are capable of insertion into the growing hydrocarbon product. The "$C_xH_yO_z$ polymerization" follows a statistical distribution known as the Anderson–Schulz–Flory (ASF) distribution, with a chain growth probably denoted as α. At higher α, the formation of larger hydrocarbon chains is favored. The value of α is depending on the active metal used in the FTS catalyst. Nickel has a low α, and will produce mostly methane, iron typically yields gasoline-range molecules, and cobalt is used for making FTS catalysts producing waxes, which can be cracked back down to desired hydrocarbons, like diesel. Pressure, temperature and H_2:CO ratio, as well as promotors can influence the chain growth probability. The products from the FTS process are almost exclusively linear alkanes and alkenes. Isomerization of the FTS products is typically performed in a separate process, although suggestions for one-pot processes also exist. These require a dedicated isomerization function to be added to the catalyst system. Specifically in nickel-based and iron-based FTS catalysts, the formation of graphitic carbon filaments is observed. These are thought to originate from the separation of carbon species from mobile (sub-)surface carbide species (see Figure 5).

The carbon filaments can grow rapidly, which may break up the catalyst particles and cause reactor plugging in multi-tube reactors. Similar carbon filaments are observed for nickel and nickel-copper catalysts for methane steam reforming (MSR) processes.[95,96] Deactivation of the Co-based low-temperature FTS catalysts (which typically have a high α, and thus produce longer hydrocarbon chains) is thought to involve polymeric and even graphenic carbon species.[97] The formation of deactivating carbon deposits on catalytically active metal surfaces is not limited to FTS, however. For example, Xie et al.[98] and Lim et al.[99] demonstrate the formation of amorphous or graphitic carbon layer on different copper-electrodes used in the electrocatalytic reduction of CO_2 to hydrocarbons.

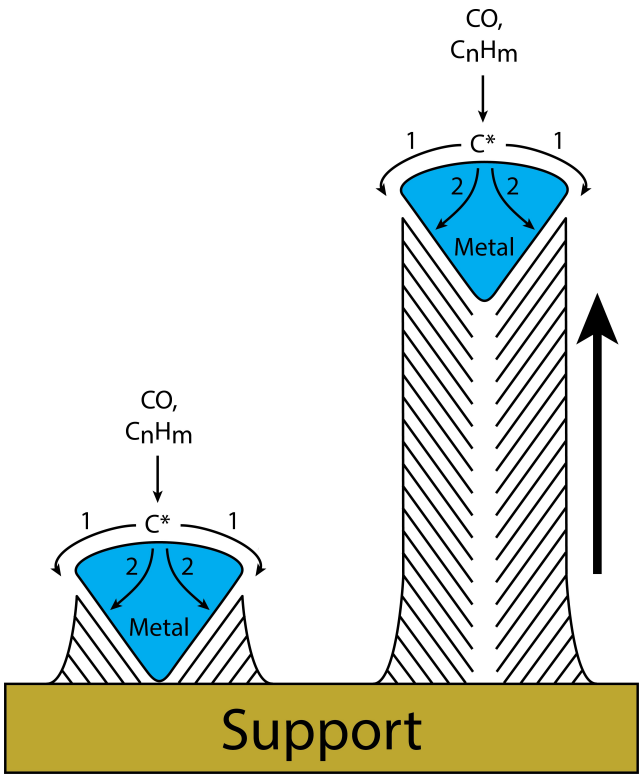

Figure 5. Formation of filamentous carbon on FTS catalyst. Surface carbon species are formed by dissociative adsorption of hydrocarbons or CO on the metal surface. These species migrate over the surface (1) or through the metal particle (2) to reach crystal facets that favor the formation of graphitic carbon layers that gradually form filaments. The left stage of this figure may be similar to the rightmost stage in figure 4. Adapted with permission from Ref. [94].

2.1.8. Direct deposition of coke from the feedstock

A final important mechanism for deactivation by coke is the direct deposition of coke (e.g., porphyrinic species or graphenic layers from asphaltenes) from the feedstock,[76,100] without the need for chemical conversion processes, such as FCC, and HPC. Coke species deposited directly from the feedstock can of course be extended by the reaction mechanisms described above, although not much detailed information is available in the literature on these processes.

2.2. Thermodynamics

It is evident from the above-described conversion processes that carbon deposits can be formed on heterogeneous catalysts in a wide variety of compositions, types and forms. Furthermore, the formation of catalytic carbon deposits in

hydrocarbon conversion processes, as a result of the conversion process, is observed under many different process conditions with process temperatures ranging from 60–800 °C, and pressures ranging from atmospheric conditions to pressures as high as 150 bar hydrogen (see Table 1).

Low-temperature conversion processes where carbon deposits play a significant role are lower olefin alkylation and olefin oligomerization. The objective of these processes is of course the oligomerization of smaller molecules, so a compromise has to be found in solid catalysts and process design (e.g., low olefin to paraffin ratio) to optimize the selectivity to the desired C_6-C_9 products.[101] In these processes, the carbon deposits probably consist of rather aliphatic polymeric species. Liu et al.[102] report that in order to limit catalyst deactivation in alkylation, the deprotonation of carbenium ions needs to be avoided, and hydride transfer (in a complex multimolecular pathway) needs to be considered as the most desirable pathway for propagation or termination of the carbenium ion pathway. At higher temperature (>250 °C) in general, dehydrogenation and especially ring closure becomes thermodynamically more favorable, and polyaromatic coke deposits are formed. Figure 6 shows the calculated Gibbs energy per carbon atoms for a variety of molecules involved in the hydrocarbon conversion processes described here. The concept of the Figure is based on Ref. [20]. Thermodynamic data for the related calculations were obtained from a variety of sources. Lower Gibbs energy represents the more stable species. The figure contains a surprisingly narrow band for arenes, which contains values for benzene, toluene, naphthalene, and anthracene. It is clear that these species are thermodynamically favored over all other hydrocarbon species above 500 °C. Above about 250 °C, cycloalkanes will dehydrogenate, for alkanes the temperature above which dehydrogenation is favored varies. The low end of the C_3-C_8 alkanes band is propane (aromatic formation is favored at 500 °C), and Gibbs energy per carbon atom increases with rising carbon number, so the high end of the band is 2,2,3-trimethylpentane (aromatic formation favored already at about 300 °C). The graph also shows the temperature ranges in which the important processes are performed. At the FCC process temperatures (i.e., 500–550 °C), the formation of (multi-)aromatic species is clearly thermodynamically favored, but even at the lower temperature at which hydroprocessing is performed, dehydrogenation of cycloalkanes to arenes is favored. Under MTH process reaction conditions, (methylated-)aromatic molecules are more thermodynamically favored than the corresponding alkene.[103,104] Moreover, the Gibbs energy of formation for amorphous carbon is lower than that for any hydrocarbon. This means the formation of multi-ring aromatics and amorphous carbon deposits is thermodynamically favored under MTH conditions.[20]

Of course, HPC and hydrocracking are performed at considerably higher hydrogen partial pressures than FCC and MTH. Nevertheless, we would expect the same behavior, with the temperature at which dehydrogenation becomes favorable depending on the pressure. In Figure 7, we present a plot of iso-equilibrium lines for the hydrogenation/dehydrogenation of benzene/cyclohexane and naphthalene/decalin as a function of temperature and pressure. We have calculated the temperature and pressure combinations at which the equilibrium composition contained equimolar amounts of hydrogenated and dehydrogenated compound (i.e., cyclohexane and benzene for the benzene hydrogenation equilibrium). It is clear the process conditions determine whether an HPC catalyst will experience a hydrogenation-favored or dehydrogenation-favored environment. Typical reaction temperatures for the HPC process are 300–400 °C. At high hydrogen pressure (>50 bar) hydrogenation will be favored over the entire temperature range, and catalytic coke formation is unlikely. However, attaining this regime requires large amounts of hydrogen, which may not be available at every refinery. At relatively low hydrogen pressure (i.e., 10–15 bar), the catalyst will be in a dehydrogenation environment or in a transition zone depending on the feedstock composition. It is known that the feedstocks with higher amounts of mono-cyclical mole-

Table 1: Catalytic hydrocarbon conversion processes where carbon deposits are a main cause of catalyst deactivation.

Process	Temp. (°C)	Pressure (Bar)	Catalyst	Deactivation
SAA	50–90	20	Zeolite (*BEA, FAU)	hours
LT-FTS	150–300	10–30	Cobalt	months
HT-FTS	330–350	10–30	Iron	weeks
HPC	300–400	15–100	CoMo(S) or NiMo(S) on Al_2O_3	years
MTG	400	20	Zeolite (MFI)	hours/days
MTO	500	1–3	Zeolite (CHA, MFI)	hours/days
Reforming	460–525	8–50	Pt alloy on Al_2O_3	months
FCC	500–550	2–3	Zeolite (FAU, MFI)	seconds
PDH(C)	575–600	0.1–1	Cr_2O_3/Al_2O_3	minutes
PDH(O)	630–650	1–2	Pt-Sn/Al_2O_3	days
MSR	500–850	30	Nickel on $CaO.Al_2O_3$ or α-Al_2O_3	years
MDA	650–800	1	Mo/ZSM-5	days

SAA: Solid Acid Alkylation (lower olefin-paraffin); LT-FTS: Fischer–Tropsch Synthesis (low temperature): HT-FTS: Fischer–Tropsch Synthesis (high temperature); HPC: Hydroprocessing; MTG: Methanol-to-Gasoline; MTO: Methanol-to-Olefins; Ref: Reforming; FCC: Fluid Catalytic Cracking; PDH(C): Propane dehydrogenation (Catofin®) (r); PDH(O): Propane dehydrogenation (Oleflex™); MSR: Methane Steam reforming; and MDA: Methane Dehydroaromatisation. Zeolites: *BEA: Zeolite Beta; FAU: Faujasite, Zeolite Y; MFI: ZSM-5, CHA: SSZ-13, SAPO-34.

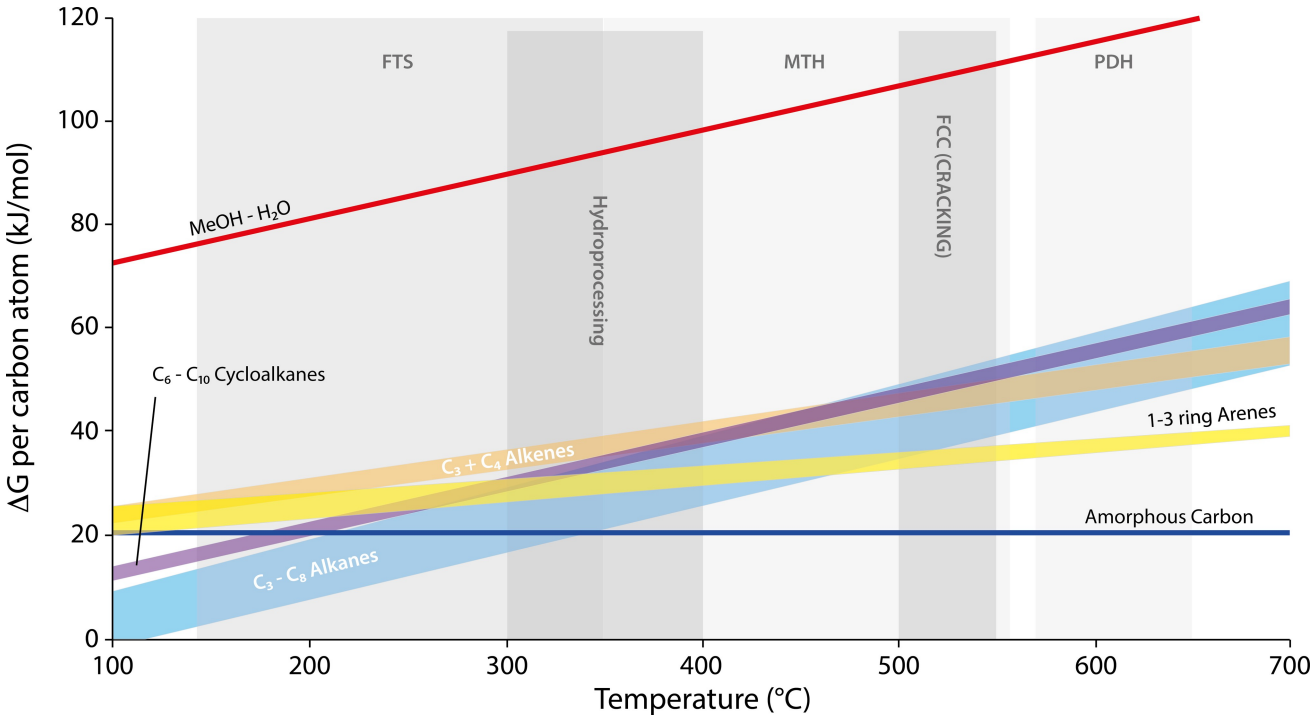

Figure 6. Gibbs energy per carbon atom at 1 bar for a variety of species involved in hydrocarbon processes. $C_3 + C_4$ alkenes: propene and 1-butene; C_3-C_8 alkanes: propane, isobutane, hexane, 2,2,3-trimethylpentane; C_6–C_{10} cycloalkanes: cyclohexane, t-decalin; 1–3 ring arenes: benzene, toluene, naphthalene, antracene. The concept of the figure is based on Ref. [20]. Original work. Copyright © 2023 the authors.

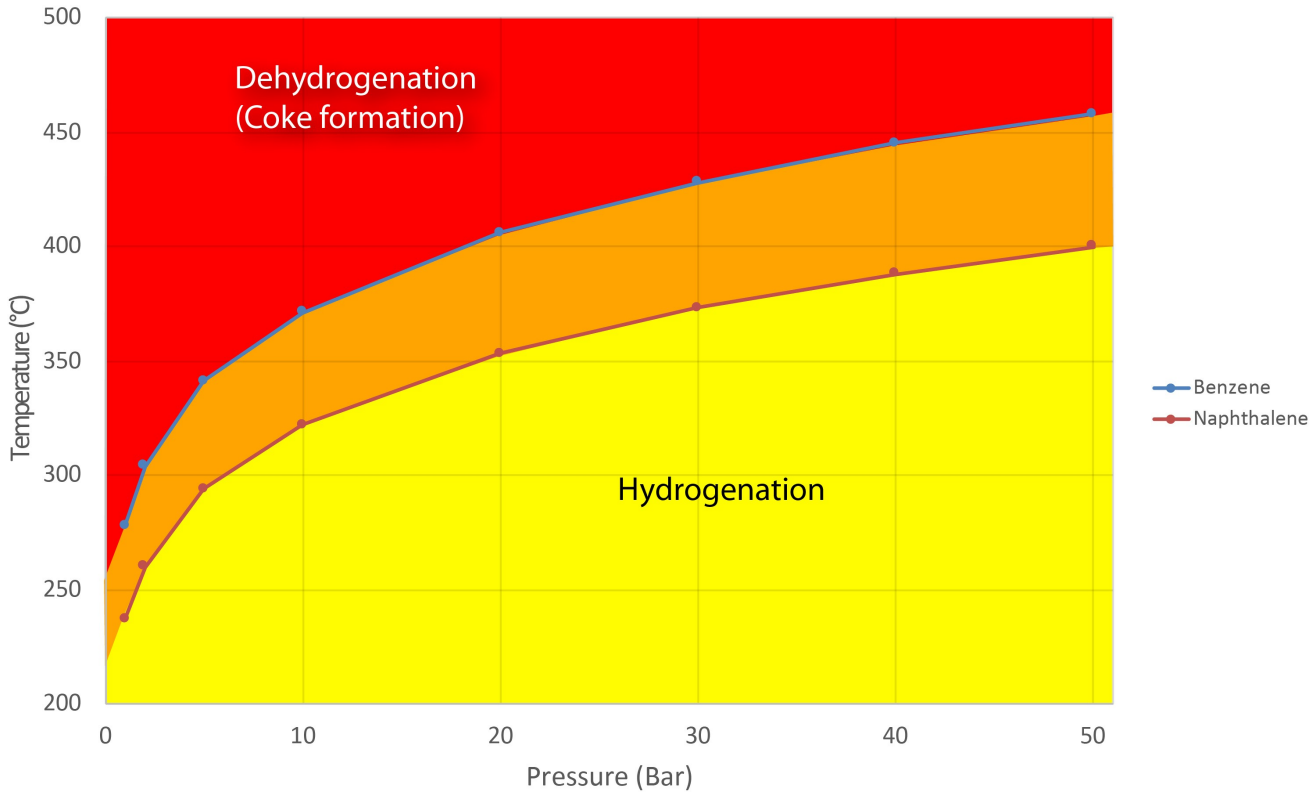

Figure 7. Iso-equilibrium curves for the hydrogenation/dehydrogenation of benzene and naphthalene. Pressure and temperature combinations were calculated for which the equilibrium conditions of the hydrogenated and dehydrogenated products were equal. In the red zone of the graph, thermodynamics favor dehydrogenation (coke formation), in the yellow zone, hydrogenation is favored. The orange zone is a transition zone. Original work. Copyright © 2023 the authors.

cules will move to the dehydrogenation zone at higher temperature, just like in FCC. The transition zone depicted in the figure is of course merely to provide an indication, the exact position and width of the zone depends on the feedstock composition.

The conclusion is that, in general, for all hydrocarbon conversion processes, even those in the presence of hydrogen, we can expect aromatic coke formation to play a role at temperature beginning at 250 °C at low hydrogen partial pressure, and up to 400 °C at higher hydrogen pressures.

2.3. The role of the catalyst material in coke formation

Although it is clear from the above paragraph that thermodynamics drive dehydrogenation and coke formation at higher temperature and low hydrogen partial pressure, we should also focus on the role of the solid catalyst in the formation of coke species. The catalyst can provide two different active sites that can promote the formation of coke, namely metal sites and acid sites. The coking mechanism described in Figure 1 is driven by hydrogen transfer from Brønsted acid sites alone, without any role for a metal site. Similar mechanisms can be constructed in which carbenium ion species are formed by hydride abstraction from an alkane on a Lewis acid site.[25] A complicating factor in zeolite-catalysed reactions is the role of the pore or cage confinement in the deactivation mechanism. The formation of immobilized oligomers or larger intermediate species can easily obstruct access to the active sites. (Noble) metal sites are directly involved in the hydrogenation/dehydrogenation equilibrium by splitting or recombination of hydrogen molecules and breaking C–H bonds. These steps can form desired part of the process design or the mechanism, which implies that mitigation procedures sometimes must compromise.

3. Different types and forms of carbon deposits

3.1. Description of carbon deposits

Carbon deposits on heterogeneous catalysts can range from relatively aliphatic oligomers formed in alkylation/oligomerization reactions to highly aromatic multi-ring graphene-like structures. In some cases (i.e., FTS, and MSR), carbon nanofibers can grow from active metal particles, which can disintegrate the catalyst particle.[105] The deposition of carbon from the feedstock can block micro- or mesopores, and thus prevent access to active sites.[28] The active sites themselves may be blocked by carbon deposits, often the result of secondary catalytic reactions on acid sites. A combination of these factors can lead to the deactivation of the catalysts over periods of seconds to even years. Figure 8 illustrates the different carbon deposits. As mentioned before Karge[19] defines coke as follows: "Coke consists of carbonaceous deposits which are deficient in hydrogen compared with the coke-forming reactant molecule(s)", while others define coke as hydrocarbons with H/C ratios of 0.3–1.[100] Coke species can be divided in various classes. Young coke is formed during the earlier stages of time on stream, and contains more hydrogen (i.e., the coke contains more aliphatic chains) than old(er) coke.[74,106] Hard and soft

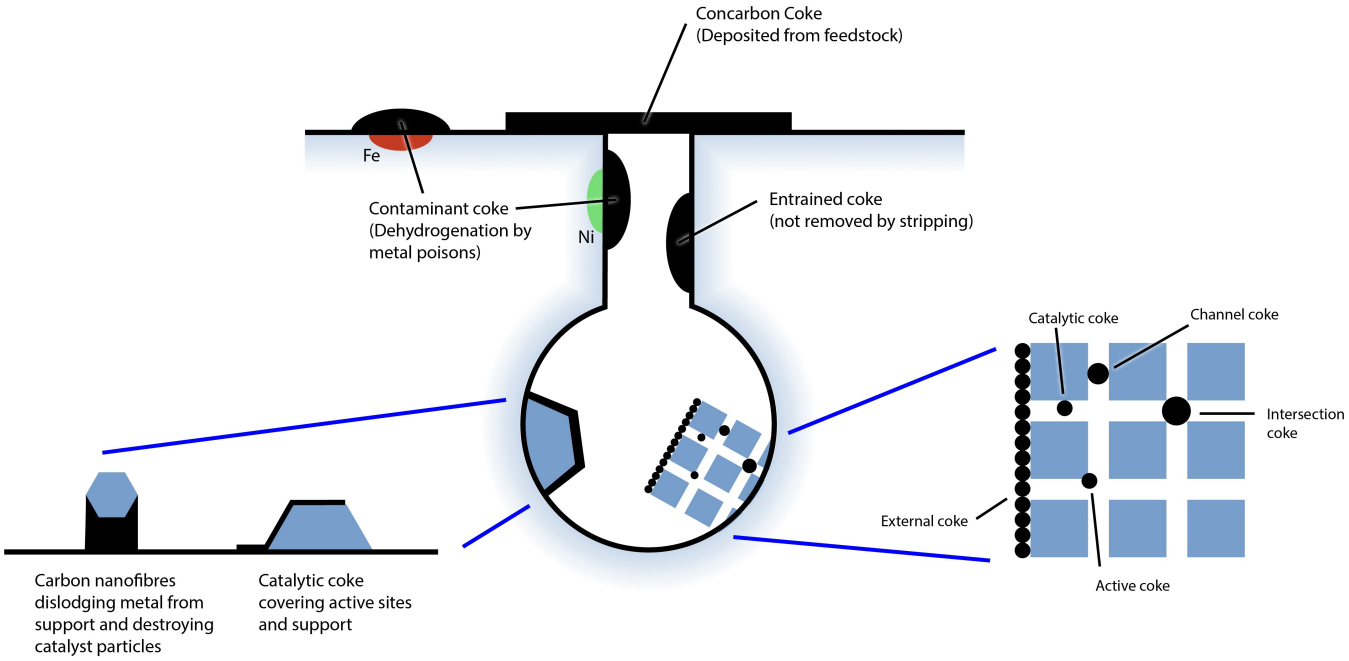

Figure 8. Different types of coke deposited or formed in catalysts during the a) fluid catalytic cracking (FCC)[100] and b) methanol-to-hydrocarbons (MTH) processes. Coke formation in hydroprocessing (HPC) catalysts is mostly limited to catalytic coke, although coke deposition from the feed may play a role in the conversion of resid feedstocks. Original work. Copyright © 2023 the authors.

coke are distinguished by their solubility in organic solvents.[107]

Cerqueira[100] et al. arrive at a total of five different coke deposits on FCC-based catalyst materials. Some of these species are directly deposited from the feedstock, and require no catalytic action, whereas others (deposited inside the catalyst particles) are formed by the catalytic process.

1) Additive coke or Conradsen Carbon Coke is deposited directly from the feedstock, and is correlated with the amount of heavy carbon species in the feedstock;
2) Cat-to-oil coke is captured in the pores and not removed in the stripper section;
3) Contaminant coke is caused by catalytic dehydrogenation on Fe and Ni species deposited on the catalyst surface;
4) Catalytic coke is a secondary reaction product of the main catalytic reaction; and finally;
5) Thermal coke, which is formed by radical mechanism at higher temperatures.

The development of coke species during the time on stream of the solid catalyst, as well as the spatial distribution of the species is likely more important than the absolute amount of coke deposited,[106] which is why it is important to design analytical strategies that can follow the spatial development of coke species over time in entire, industrially relevant catalyst particles.

3.2. Bad coke versus good coke deposits

Although the formation of coke deposits may deactivate and even disintegrate the catalyst material, not all coke species are necessarily unwanted.[106,108–111] The so-called selectivation by deposits of graphitic carbon on the exterior of the zeolite particles is known to greatly enhance the selectivity in selective toluene disproportionation[112] (e.g., ExxonMobil's PxMax^{SM} process) or ethylbenzene disproportionation.[113] Coke species deposited on the catalyst surface may even provide active sites themselves in processes, such as oxidative dehydrogenation of ethylbenzene or butane, and ammoxidation.[108] In the FTS process, at least with iron-based catalysts, an iron carbide species is assumed to be the active phase, although its exact nature is still a matter of debate.[90–93] The carbon fibers that grow as a nuisance in the FTS synthesis can be produced on-purpose to supply interesting catalyst supports.[114,115] Finally, in the FCC process, part of the coke deposited on the catalyst in the cracking stage is burnt off in the regenerator reactor to yield the heat required to run the process.[25] Similar coke formation phenomena are taking place in the PDH process, which, like the FCC cracking step, is also endothermic in nature.

Heavy coke has been generally accepted as the primary cause of the deactivation of zeolite-based catalyst materials. However, the selectivity of a complex reaction, such as the MTH process, can be affected by the coke formation depending on the type of zeolite framework topologies.[116] For small pore, cage-type zeolites, like HSAPO-34, the internal coke species accumulated in the CHA cages are responsible for the deactivation of the catalyst.[117] Meanwhile, a gradual increase of ethylene to propylene ratio was observed with the accumulation of the coke species in HSAPO-34 molecular sieves.[72,118] Holmen et al. attributed the change of selectivity to the decline of pore volumes due to coking that varies the transition-state shape selectivity of HSAPO-34.[116,119] In contrast, for channel-type zeolite HZSM-5 or one dimensional zeolites, it has been found that the catalyst selectivity is independent on the coke deposition.[120] This could be due to the fact that the deactivation of channel type zeolites is caused by the external coke species that covers the surface of zeolites.[103,117] In this case, the internal structure of the zeolites is not significantly changed by coke species. In the dry reforming of methane (DRM), Wang et al.[111] propose a specific role in the reaction mechanism for some of the coke species that are oxidized to CO to contribute to the process yield.

4. Analysis of carbon deposits

4.1. Classical analytical methods

The early stages of coke formation, as described above, concern relatively small species that can be observed directly using in situ or operando techniques using e.g., IR-spectroscopy, but the majority of the species observed in more advanced deactivation concerns polyaromatic species that require other techniques. In essence progressing coke-formation proceeds from the left-top region in Figure 9 to the lower right regions, During this process, the catalysts rapidly turn black, limiting the applicability of optical or IR spectroscopy especially in transmittance mode. Raman spectroscopy does not suffer from this problem, although fluorescence may be an issue.

Temperature Programmed Oxidation (TPO) is one of the most widely used analytical techniques. It provides direct information regarding coke oxidation rate, which provides significant information for the design of regeneration processes of the catalysts. In addition, it is possible to obtain useful information, such as location, composition (hydrogen/carbon ratio), coke amount, and morphology.[121] The information regarding coke oxidation kinetics is relevant to properly design regeneration processes of solid catalysts. It can be performed using different detection methods, e.g. differential thermal analysis (DTA) and thermalgravimetric analysis (TGA). Transmission electron microscopy (TEM) is often used to study the localization, nature and structure of coke deposits. Electron energy loss spectroscopy (EELS) is normally attached to TEM to obtain qualitative information regarding the type of coke present with high spatial resolution of 1 nm^2.[122] Infrared (IR) and Raman-spectroscopy are powerful tools to study the chemical identity of the chemical compounds that form the coke deposits, such as olefinic, saturated or aromatic.[86,123] Additionally, information regarding the location of coke can be obtained by following the signal of certain catalyst surface groups, such

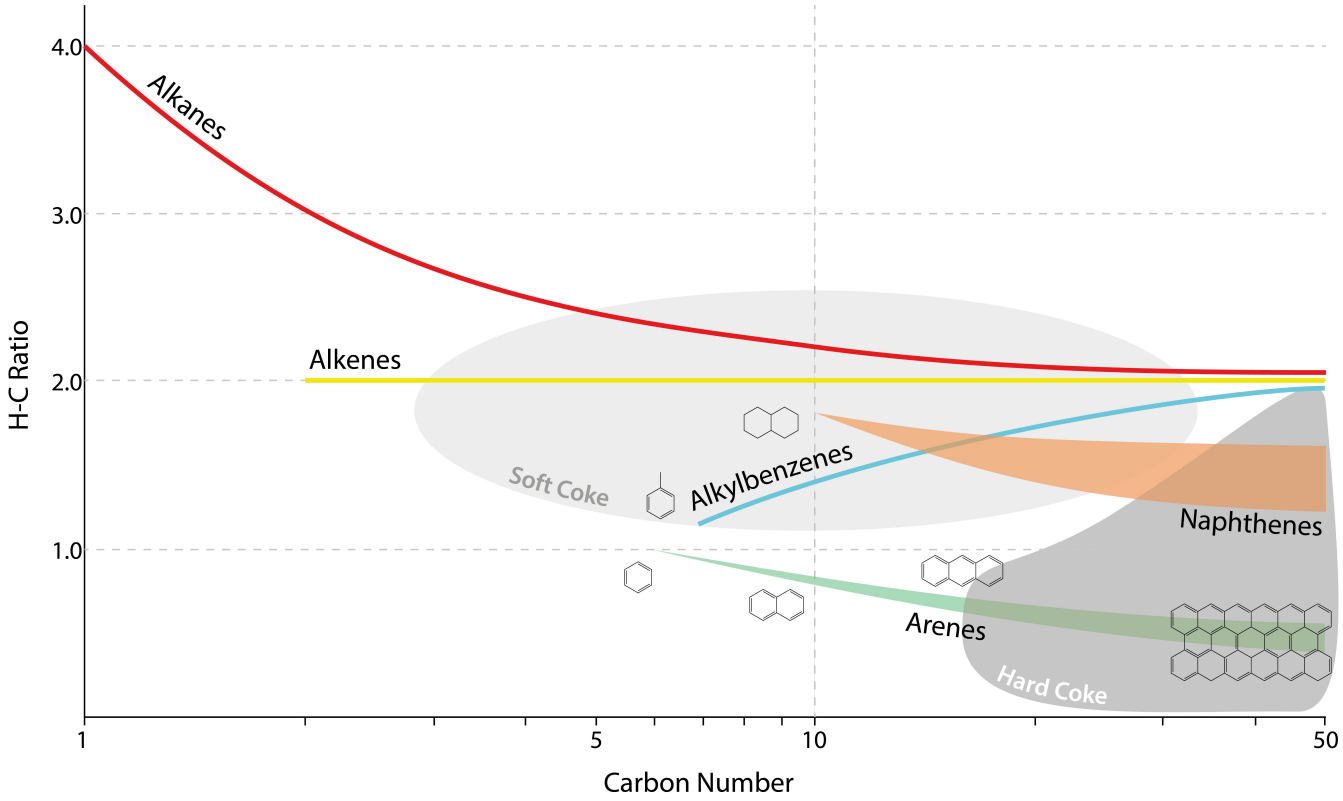

Figure 9. Various carbon species. Coke formation directionally moves reactants from the left top to the right bottom, but species in the middle of the plot can also be coke (intermediates). Original work. Copyright © 2023 the authors.

as Bronsted OH.[124] In a conventional approach, Guisnet and Magnoux[28] dissolve the coked catalyst (component) in a solution of 40 % HF to isolate the coke. The concentrated coke can then be characterized with more or less standard techniques (i.e., soluble species can be studied with gas chromatography (GC), high-pressure liquid chromatography (HPLC), NMR, insoluble species with solid-state NMR, TEM and EELS). This analytical approach of course destroys all information on the solid catalyst, and makes it impossible to correlate the formation of coke species with catalyst features.

4.2. Advanced analytical methods as demonstrated with a selection of showcases

Although classical analytical methods have offered a wealth of bulk-averaged fundamental knowledge,[19,28] fully understanding the deactivation of e.g. zeolite-based catalysts requires characterizing sub-nanometer length scales of the atomic bond to real reactors due to the intricate heterogeneities in space for catalysis.[125] A single method is rarely sufficient to fully understand the complex interplay of processes occurring at different length- and timescales.[126] A variety of (operando) characterization tools with high spatial resolution has been used over the last decade to study the coke species formed or deposited. For example, Guisnet et al. describe how carbon species can be extracted from the catalyst and analyzed ex situ e.g. with ^{13}C-MAS-NMR.[127] On the other hand, Fonseca et al.[74,128,129] use the same tool to study the speciation of carbon on HPC catalysts (i.e., not extracted) with higher coke-loading. The bulk analytical techniques, as partially mentioned above, described encompass TPO/TGA,[130] ^{13}C NMR,[74,113,128,129,131–133] (FT-)IR,[19,28] UV/Vis,[134,135] NEXAFS,[136–138] EELS,[139,140] EPR,[28,113] PET,[141,142] XPS,[132,140] and MALDI-TOF/MALDI-FT-ICR-MS.[22,143] Spatial resolution of coke species was studied with among others APT,[144] STXM,[145,146] SEM,[147] TEM,[105,140] in combination with EDX and EELS[122,139,148,149] and confocal fluorescence microscopy (CFM).[135] The extended polyaromatic structures can be visualized with STM and AFM[150] (see Table 2, which also contains the names for the abbreviations used for the different analytical tools available).

4.2.1. Fluid catalytic cracking process

Recently new microscopy and spectroscopy tools[158–163] have been described that allow the study of the deactivation process over time, spatially resolved to the 20–50 nanometer range, for instance in FCC catalysts, as summarized in Figure 10–12. Confocal fluorescence microscopy (CFM) and Raman spectroscopy in combination with ^{13}C-MAS-NMR can yield information on the formation of small carbon species during the initial stages of deactivation.[134,144] Differ-

Table 2: Analytical tools for the analysis of carbon deposits on solid catalysts.

	Deactivation stage		Refs.
TPO/TGA	Late	Bulk	[121,130]
TEM/SEM/EDX/EELS	Any	Atomic	[105,122,139,140,147–149]
^{13}C-MAS-NMR (DNP)	Late (high amount of coke required)	Bulk (surface with DNP)	[28,74,113,128,129,131–133]
(FT-)IR	Early/operando	Micrometer	[19,28,123,124]
UV/Vis	Early/operando	Micrometer	[134,135]
NEXAFS	Late	Bulk	[136–138]
EPR	Late	Bulk	[28,113]
PET	Late	Bulk	[141,142]
XPS	Any	Surface	[132,140]
MALDI-TOF-MS, MALDI-FT-ICR-MS	Late	Molecular	[22,143,151]
APT	Any	Local/nm	[144]
STXM	Late	nm	[145,146]
CFM	Operando	100 nm	[135]
STM/AFM	Any	Atomic	[150]
AFM-IR (PiFM)	Any	Atomic	[152]
Time-gated Raman	Early	Bulk	[153,154]
X-ray (nano)tomography	Late	10 nm	[155]

TPO/TGA: Temperature Programmed Oxidation/Thermogravimetric Analysis; TEM/SEM/EDX/EELS: Transmission Electron Microscopy/Scanning Electron Microscope/Energy Dispersive X-Ray Analysis/Electron Energy Loss Spectroscopy; ^{13}C-MAS-NMR (DNP): ^{13}C-Magic Angle Spinning Nuclear Magnetic Resonance Spectroscopy (Dynamic Nuclear Polarization); (FT-)IR: (Fourier Transform) Infrared Spectroscopy; UV/Vis: Ultraviolet/Visible light Spectroscopy; NEXAFS: Near Edge X-Ray Absorption Fine Structure; EPR: Electron paramagnetic resonance spectroscopy; PET: Positron Emission Tomography; XPS: X-ray Photoelectron Spectroscopy; MALDI-TOF-MS: Matrix Assisted Laser Desorption Ionization Time of Flight Mass Spectrometry; MALDI-FT-CIR-MS: Matrix Assisted Laser Desorption Ionization Fourier-Transform Ion Cyclotron Resonance Mass Spectrometry; APT: Atom Probe Tomography; STXM: Scanning Transmission X-ray Microscopy; CFM: Confocal Fluorescence Microscopy; STM/AFM: Scanning Tunneling Microscopy/Atomic Force Microscopy; AFM-IR (PiFM): combined Atomic Force Microscopy-Infrared Spectroscopy (Photoinduced Force Microscopy).

ent X-ray absorption spectroscopy (XAS) methods can be used to study the valence and coordination of several elements in the catalysts in one experiment, yielding (spatially resolved) information on the effects of metal poisoning,[156,164–166] changes in active species morphology,[45] and their effect on coke species. Probe reactions combined with spectroscopy can yield invaluable information on remaining activity at the active sites of the catalyst material,[167] or on the accessibility of the catalyst system.[157,168] The overall deactivation of catalyst materials is usually a combination of factors, which also implies that a variety of tools is required to fully understand the deactivation mechanism.[126,169] Element-specific X-ray microscopy (XRM) was used by Meirer et al. to analyze the 3D distribution of deactivating metals, like nickel and iron, in (post-mortem analysis of) several stages of FCC catalyst age.[156,170] Both iron and nickel are related to carbon formation, firstly because they deposit with or from porphyrin-type species and second because they can be converted into hydrogenation/dehydrogenation catalytic sites, which alter the catalytic performance of FCC particles. Apart from the precise location of the metals, to 3D network of the pore system could also be visualized for entire FCC particles using FIM/SEM tomography[171] or X-ray Tomography,[126,156,170] and effects of pore blockage could be modeled using resistance networks similar to electrical circuits.[126] Using fluorescent probes, the diffusion of VGO-like molecules could be visualized, which further enhanced the fundamental understanding of the pore system of entire FCC particles.[157] Recently the work was expanded by a study in which low Z-low contrast carbon was visualized directly using 3D X-ray nanotomography in the analysis of one single FCC particle before and after calcination.[155] With this innovative methodology, it was possible to observe dense coke species on the outer surface of the catalyst, in direct proximity of iron (as identified and localized by XRF tomography), and a lower density of coke species inside the FCC particle. The presence of coke species, but not their speciation, had been demonstrated by X-ray ptychographic tomography before by van Bokhoven and co-workers.[172]

The result of the 3D X-ray nanotomography work by Veselý et al.[155] confirmed earlier observations from DNP-enhanced ^{13}C-MAS-NMR experiments by Mance et al., in which they showed[131] that aromatic carbon species (feedstock coke) dominate on the outer surface of FCC catalysts, and are in proximity to iron deposits, which were identified with EPR, and localized with the SEM-EDX technique. More aliphatic coke species (catalytic coke) were found in the interior of the FCC particles. The workflow involved performing 3D X-ray holotomography on a single FCC particle before and after calcination, followed by XRF tomography to establish the spatial distribution of elements, like Ni and Fe. In the data analysis, the 3D information of the three experiments could be overlaid to yield a visualization of the (disappearance of the) coke species, and a correlation of the spatial distribution of the coke with the metals distribution.[155] In a recent paper, Alabdullah et al. described the direct cracking of crude oil to chemicals using FCC-like catalyst materials.[173] They conclude that zeolite degradation is the main reason for catalyst deactivation and suggest that the role of metals and coke is minimal. However, the authors work at very low metal concentrations

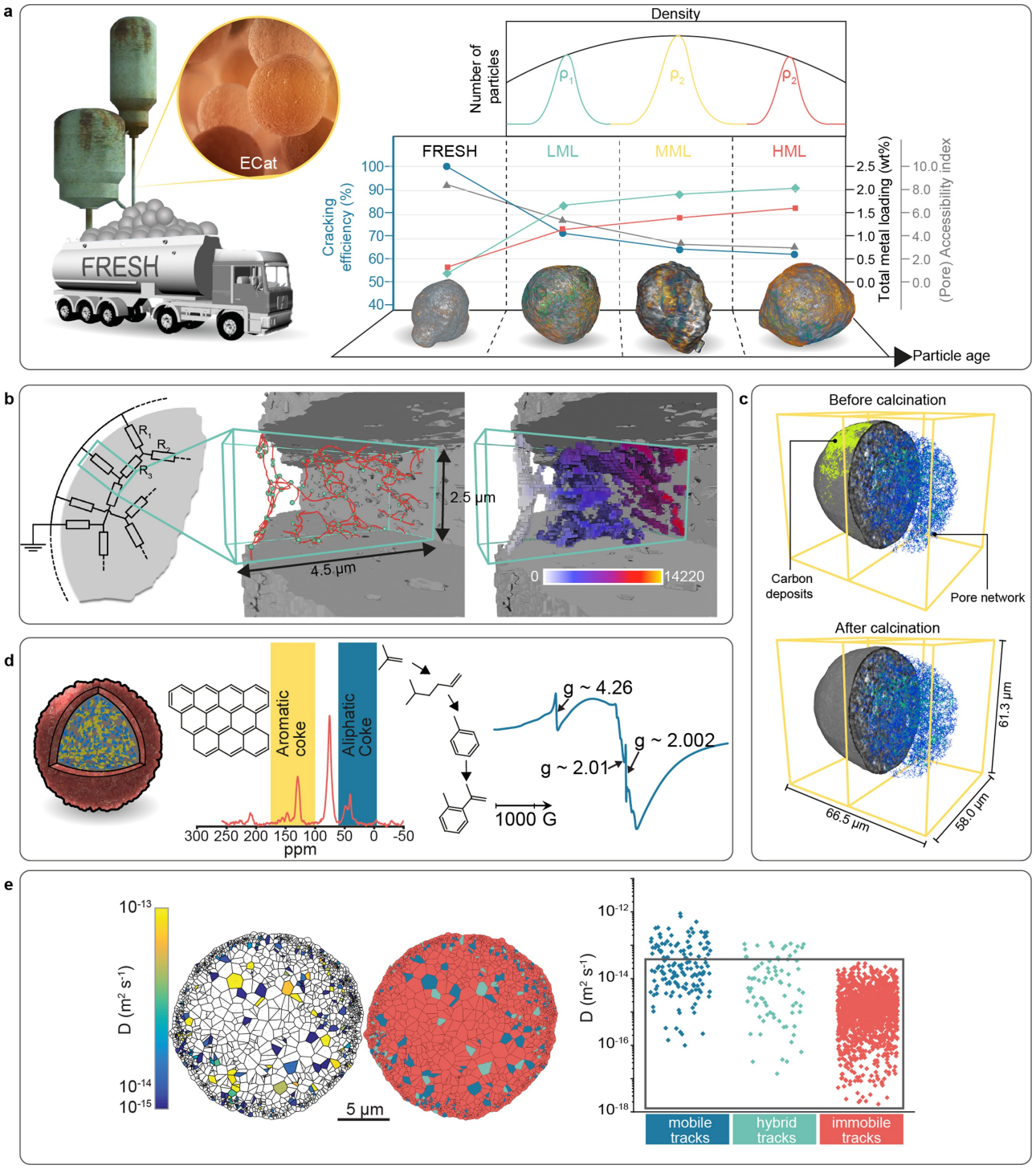

Figure 10. An overview of recent techniques for the study of coke on fluid catalytic cracking (FCC) catalysts. Panel A: The distribution of various metals through the FCC particle as a function of age was studied by X-ray holotomography (reproduced from Meirer et al.,[156] under the terms and conditions of the Creative Commons CC-BY 4.0 license. Copyright © 2015 the authors). Panel B: Pore structure information from X-ray tomography was used to model the diffusion (reproduced from Liu et al.,[126] under the terms and conditions of the Creative Commons CC-BY 4.0 license. Copyright © 2016 the authors) Panel C: The direct proximity of coke and iron species was directly demonstrated in a combination of X-ray holotomography and micro-X-ray fluorescence (XRF) (reproduced from Veselý et al.[155] under the terms and conditions of the Creative Commons CC-BY 4.0 license. Copyright © 2021 the authors) Panel D: left: an FCC particle, with various functionalities spread through the spherical particle, right: Dynamic nuclear polarization (DNP) magic angle spinning (MAS) ^{13}C nuclear magnetic resonance (NMR) was used in combination with electron paramagnetic resonance (EPR) to demonstrate the proximity of iron and coke species (Reproduced with permission from Mance et al.,[131] Copyright © 2017 The Royal Society of Chemistry). Panel E: Single particle fluorescence microscopy was used to track the diffusion of vacuum gas oil (VGO)-like probes in an FCC particle (reproduced from Hendriks et al.,[157] under the terms and conditions of the Creative Commons CC-BY-NC-ND license. Copyright © 2017 American Chemical Society.

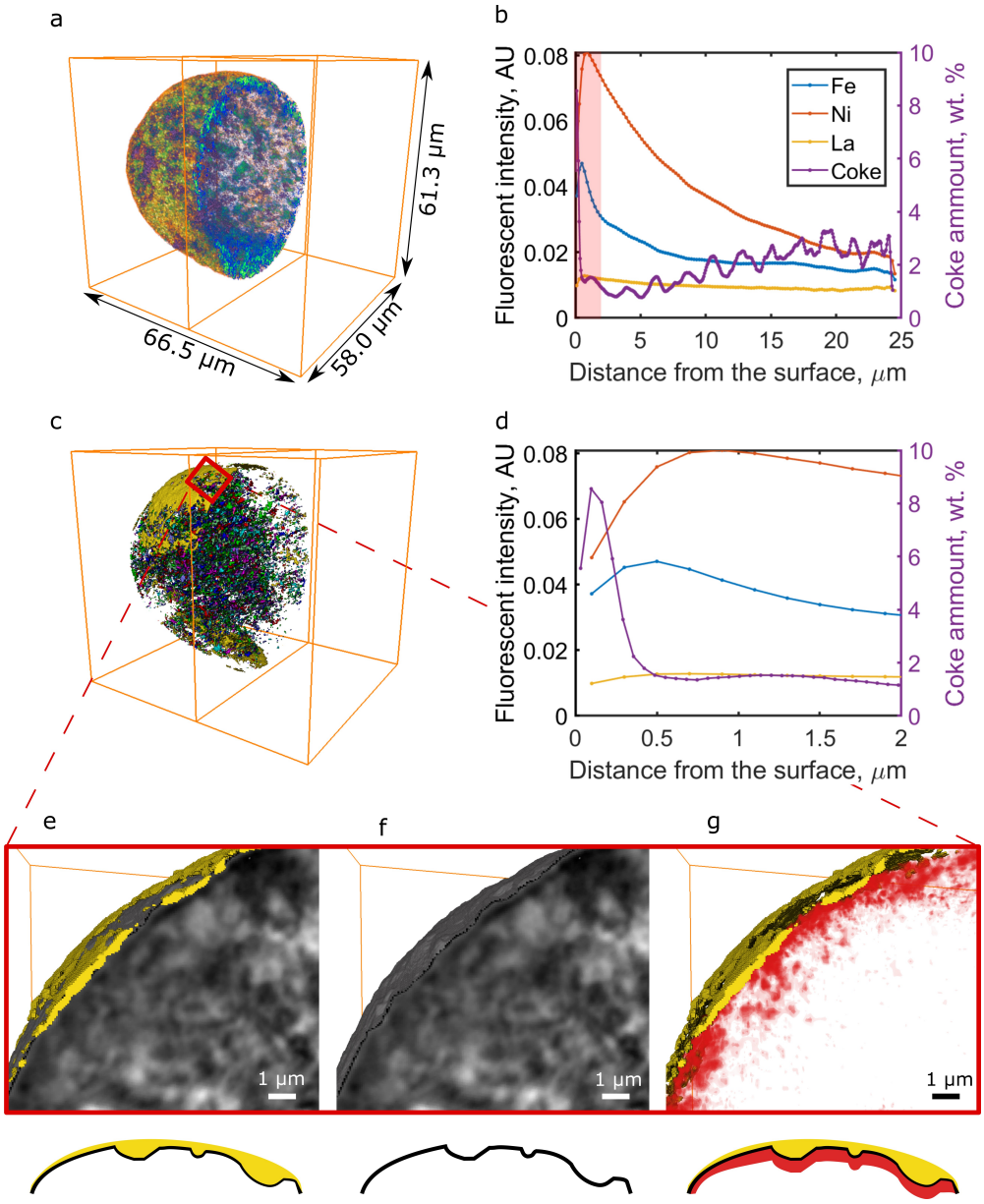

Figure 11. Correlated 3D distributions of carbon deposits and metals from X-ray fluorescence (XRF) tomography and hard X-ray holotomography. (a) 3D distribution of iron (yellow-red), nickel (blue-green), and lanthanum (magenta). (b) Radial profiles showing relative concentrations of iron, nickel, lanthanum, and carbon as a function of distance to the surface. (d) Zoom in to the 2 µm surface region revealing a large amount of carbon deposited on the catalyst particle's surface. (c) 3D distribution of individual carbon deposit clusters (individual clusters are plotted in different colors). (e) A zoom into the near-surface region of the catalyst particle shows the catalyst particle (grey) and one of the large surface carbon deposit clusters (yellow). (f) Patchy surface carbon clusters smoothen the nodulated surface of the particle (see also the sketch below panels e–f). Panel (g) correlates the 3D Fe concentration distribution with the surface carbon cluster, demonstrating that dense surface coke species are located in close vicinity to Fe found close to the surface of the catalyst particle. Reproduced from Veselý et al.[154] under the terms and conditions of the Creative Commons CC-BY 4.0 license. Copyright © 2021 the authors.

compared to the works presented above and use completely different reaction/regeneration cycles (each 4 h, at 570 °C and 800 °C, respectively) compared to FCC, which implies their seemingly contradictory conclusions cannot be readily compared to the body of work described above.

Additional structural information on coke species could possibly be provided by carbon K-edge Near Edge X-ray Absorption Fine Structure spectroscopy (NEXAFS), as demonstrated by Bare et al. for reforming catalysts.[169] Shimada et al.[136] report the use of this technique for the analysis of coke species on various catalyst systems, like DRM, HPC, and FCC catalysts. They conclude that, unlike NMR, this technique can be used to observe the highly graphitic coke species relevant for the later stages of deactivation. Smith and Lobo[137] have used the same technique to study carbon species formed in SBA-15.

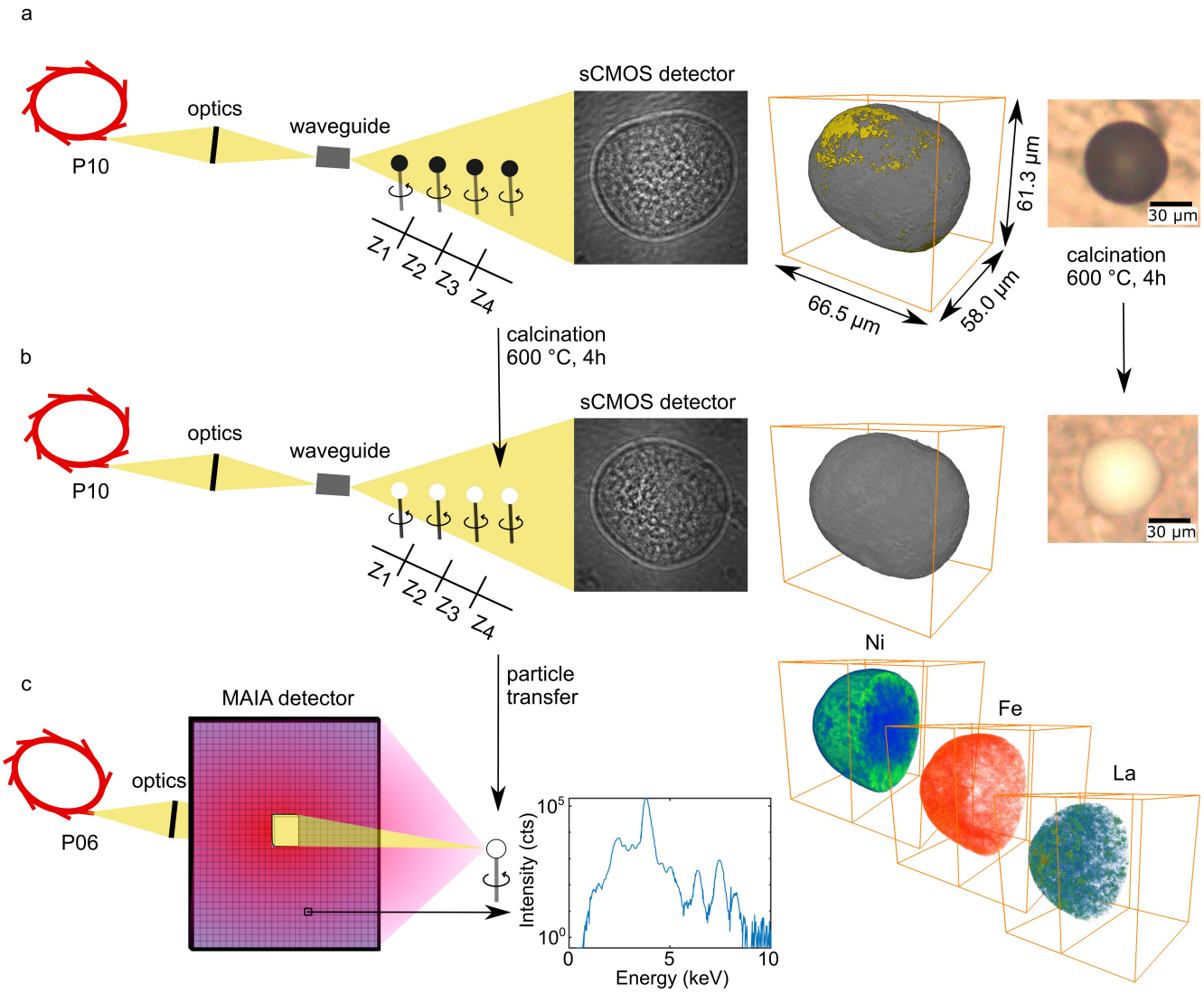

Figure 12. Experimental workflow and detection Schemes. (a) X-ray holotomography was performed on an equilibrium fluid catalytic cracking (FCC) particle mounted on a carbon tip. Tomography was performed at four different distances between sample and scintillator-based fiber-coupled sCMOS detector. (b) After the first measurement, the particle was calcined to burn off coke deposits. The particle was then re-mounted and measured again with X-ray holotomography. (c) After this second X-ray holotomography the catalyst was also imaged by X-ray fluorescence (XRF) tomography. XRF spectra were fitted to quantify the relative concentrations of the detected elements in every single pixel and at each projection angle; In the final step 3D representations of the sample's electron density as well as the 3D distribution of coke deposits (in yellow in (a)) have been reconstructed from X-ray holotomography, and the 3D distribution of specific elements of interest has been reconstructed from XRF tomography. Reproduced from Veselý et al.[155] under the terms and conditions of the Creative Commons CC-BY 4.0 license. Copyright © 2021 the authors.

NEXAFS, like EELS, detects the transitions of inner shell electrons to unoccupied orbitals. Both techniques can therefore in principle provide useful information on the presence and type of aromatic species. The interpretation of the spectra is, however, not easy and requires modeling to provide additional information. Oji et al.[174] demonstrate the simulation of NEXAFS spectra for specific polyaromatic species in support of NEXAFS analysis.

The new tools have thus provided insights in the early stages of the deactivation process, and have greatly enhanced our understanding of the chemistry and location of metal poisons, and the deactivation of the zeolites inside the catalysts. Enhanced 3D visualization and network analysis of the pore system during deactivation, combined with direct observation of molecules diffusing and reacting have provided new insights in the role of accessibility in FCC. The distribution of different coke species (directly deposited from feedstock and catalytic coke) was demonstrated with DNP-NMR, and then visualized directly with X-ray holotomography. Finally, the tools allowed for spatial correlation of the various species involved in deactivation.

4.2.2. Methanol-to-hydrocarbons process

Mores et al.[134,135] studied the early stages of coke formation on the zeolites used in the in the MTH process. They have investigated large crystals of zeolite HZSM-5 (with the MFI topology) and HSAPO-34 (with the CHA topology), and visualized the formation of coke precursors, in this case relatively small species that typically fit in the micropores of the zeolite structures, as a function of time and temperature in 3D using multi-laser excitation confocal fluorescence microscopy and UV/Vis-NIR micro-spectroscopy. Larger polyaromatic structures typical for later stages of the deactivation process were addressed in a subsequent paper of the same group.[175] These studies show that "large" coke species form within the straight channels, eventually reaching and covering the external surface of the zeolite HZSM-5 crystal.[134,135] Wei et al.[176] observed adamantane species during the induction period at low temperatures (300–325 °C) in SAPO-34. Wang et al.[143] observe the fingerprints of polyaromatic hydrocarbons with Fourier-transform ion cyclotron resonance mass spectrometry (MALDI FT-ICR MS), and conclude the detailed knowledge obtained of the molecular nature of the PAH's provides options for the optimization of the coking/decoking process steps. An earlier paper by the same group had already provided indications for the role of cage-passing polyaromatic hydrocarbons in the transition from soluble to insoluble coke species.[177]

Sprung et al.[178] extended the single component studies of Mores et al. to full catalyst systems, by studying FCC catalysts, and managed to visualize the 3D-distribution and orientation of HZSM-5 crystals within FCC catalyst particles, again using the CFM technique.[179] Qian et al.[73] have studied the MTH-reaction intermediates and coke precursors using combined operando UV/Vis/NIR spectroscopy.

Zeolite deactivation in the MTH process has been studied using numerous approaches, including the use of theoretical models,[103,104] spectroscopic techniques and kinetic investigations.[54,56,68,70,134,144,180] By comparing the Gibbs energy of formation per carbon for the reactant and product molecules, Olsbye et al.[20] showed that the formation of arene and alkane species are more thermodynamically favorable compared to the alkene species during the MTH process. Moreover, the Gibbs energy of formation for amorphous carbon is lower than for any hydrocarbon (see Figure 3, based on the work of Olsbye et al.). This means that all these hydrocarbons may ultimately be transformed into amorphous carbon under the MTH conditions.[20] A recent study correlates coke species deposition and formaldehyde evolution, that is also involved in the first C–C formation.[56] Reacting with olefins via a Prins approach, formaldehyde predominantly converts to H-poor molecules, i.e., dienes, aromatics and coke species. The same group also pointed that this reaction requires Lewis acid sites.[54] Studies demonstrated that the deposition of coke species is responsible for the deactivation of zeolite crystals and that the deactivation is a complicated process.

To establish a complete picture of zeolite deactivation, the coke formation during/after the MTH process at different length scales from nanometer to full catalyst bed were studied in the Weckhuysen group, illustrated in Figure 13. Atom Probe Tomography (APT) has been demonstrated to be a powerful analytical method to identify the affinity between Brønsted acid sites (Al^{3+} for HZSM-5, Si^{4+} for HSAPO-34) and clustering of coke species with a median size of 30–60 ^{13}C atoms, that are believed to likely be the first coke precursors leading to pore blockage and subsequent deactivation.[144,185–188] The deactivation behavior during the MTH process has also been studied at the level of single oriented channels by combining a well-designed model system, i.e. uniformly-oriented zeolite HZSM-5 thin-films, and operando UV/Vis diffuse reflectance spectroscopy (DRS) coupled with online mass spectrometry (MS).[189] With the ability to decouple the active zeolite channels, the oriented thin films allowed the researchers to follow the products produced within single oriented channels. It has been observed that toluene was formed in the sinusoidal zeolite channels, while it was absent in the products from the straight zeolite channels. Simultaneously measured UV/Vis DRS data illustrated that the straight zeolite channels favor the formation of internal coke species, leading to pore blockage and thereby explaining the absence of aromatics in the product stream. In contrast, the oligomerization of aromatics is suppressed within the sinusoidal zeolite channels, and toluene can easily diffuse out and further grow into e.g., polyaromatics on the corresponding zeolite outer surface. Similar results were also obtained using a large zeolite HZSM-5 crystals (ca. $100\times20\times20\ \mu m^3$) with the combination of either in situ UV/Vis DRS or confocal fluorescence microscopy techniques.[134,135] It is concluded that the internal coke species formed in the straight zeolite channels could further growth and cover the external surface of the zeolite HZSM-5 crystal. Extending the information gained from the zeolite thin-films to anisotropic zeolite crystals unambiguously demonstrated that the deactivation of zeolite ZSM-5 during the MTH process is dictated by the external coking. Using DNP-NMR spectroscopy and well-synthesized anisotropic zeolite crystals, Fu et al. showed that heavy coke species are prone to grow at the surface connecting to sinusoidal channels of HZSM-5.[190] By combining operando UV/Vis and IR spectroscopies, Qian et al.[73] found that polyaromatic species could block the pore of HSAPO-34 zeolites and leads to the deactivation for the MTH process. Research has also focused on the larger scale of the crystal level to determine the magnitude and direction of the zeolite lattice expansion during the MTH process. Obvious expansion along the *c*-axis of the lattice of CHA was observed in the studies from various groups.[53,184,191–193] Goetze et al.[184] analyzed the hydrocarbons that cause the lattice expansion of zeolite cages with different topologies by the combination of operando XRD (as also used by Rojo-Gama et al.[183]) and UV/Vis spectroscopy. They found that methylated naphthalene and pyrene, 1-methylnaphthalene as well as methylated benzene and naphthalene are the coke species leading to cage expansions in CHA, DDR and LEV zeolites, respectively. Studies of HZSM-5 zeolites show that differences between the lengths of the *a*- and *b*-unit cell vectors decrease with increasing

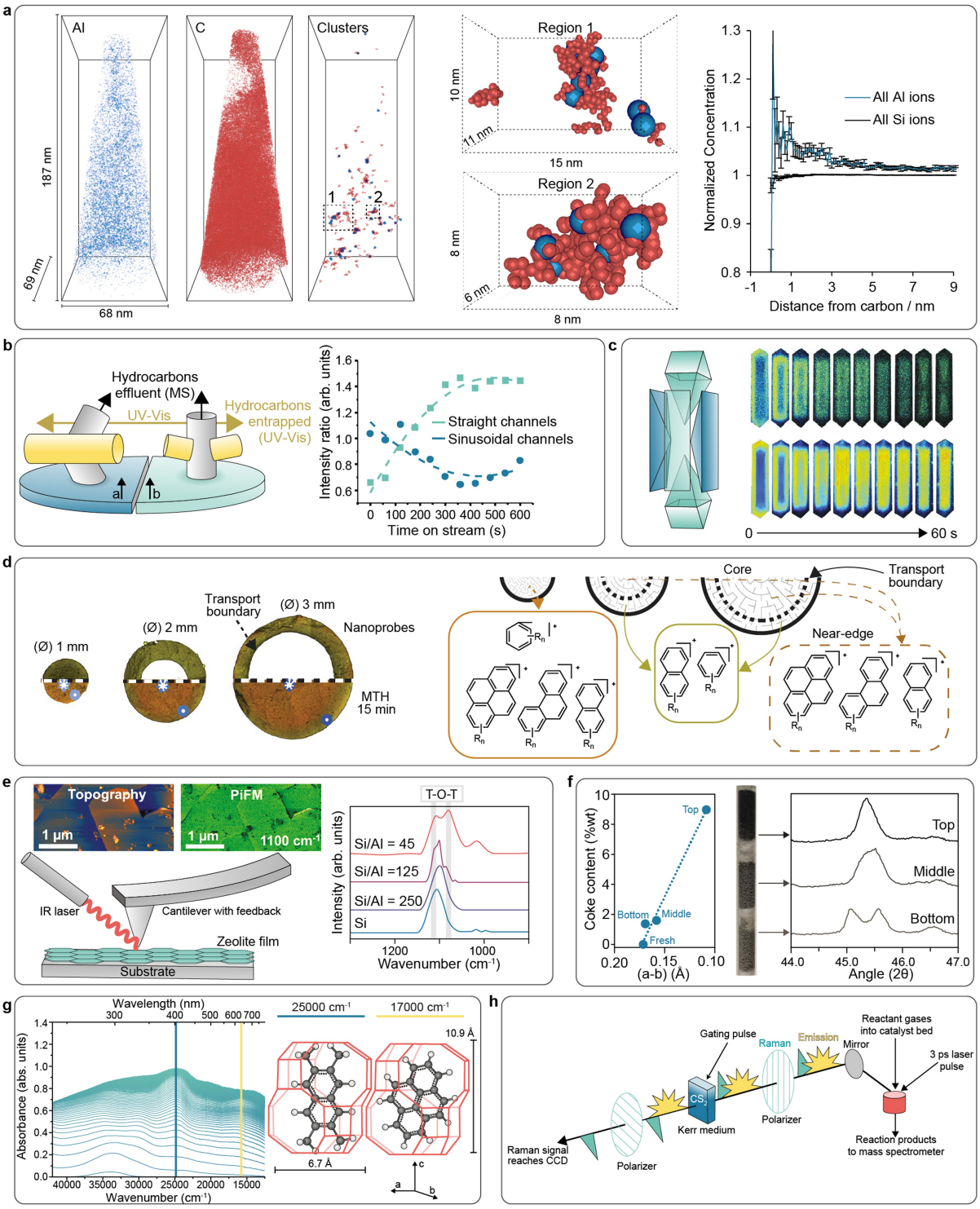

Figure 13. An overview of recent techniques for the study of coke on methanol-to-hydrocarbons (MTH) catalysts. Panel A: Atomic resolution information on the distribution of coke was obtained from atom probe tomography (APT) (reproduced with permission from Schmidt et al.,[180] Copyright © 2018 Wiley). Panel B: Information on the coking mechanism was obtained from studies on oriented layers of zeolite ZSM-5 crystals (reproduced from Fu et al.,[181] under the terms and conditions of the Creative Commons CC-BY-NC 4.0 license. Copyright © 2017 the authors). Panel C: Fluorescence microscopy on isolated large zeolite ZSM-5 crystals was studied by Mores et al.[135] (reproduced with permission, Copyright © 2008 Wiley). Panel D:Whiting et al.[182] used confocal fluorescence microscopy (CFM) to study entire catalyst extrudates (reproduced with permission, Copyright © 2018 the authors). Panel E: Photo-induced forced microscopy (PiFM) was used by Fu et al.[152](reproduced with permission, Copyright © 2017 Royal Society of Chemistry). Panel F: X-ray diffraction (XRD) of coked zeolites was performed by Rojo-Gama et al.[183](reproduced with permission, Copyright © 2017 American Chemical Society). Panel G: right: The catalyst (i.e., a CHA-zeolite) with reactant molecules in the cages, left: Operando UV/Vis results on this catalyst system (reproduced from Goetze et al.[184] under the terms and conditions of the Creative Commons CC-BY-NC-ND 4.0 license. Copyright © 2018 American Chemical Society). Panel H: The separation of the Raman signal and the fluorescence signal in operando time-gated Raman spectroscopy (original image based on Greetham[154] and Lezcano-Gonzalez et al.[153]).

deactivation.[183] More recently, differences in external coke species between the two crystal planes were observed, which was attributed to the differences in the diffusion properties of the straight and sinusoidal channels resulting from different coke precursor diffusion and different coke deposition.[122] Lezcano-Gonzalez et al.[153] used operando Kerr-gated Raman (or time-gated-Raman) spectroscopy to study the formation of catalyst-deactivating polycyclic aromatics, and conclude a crucial role is played by polyenes, for which formation and ultimate destiny is determined by their confinement in the zeolite structure. The reaction behaviors of the MTH process were also studied at the reactor scale using both theoretical and experimental approaches. Three zones, namely the initiation, autocatalytic and product zone, were observed from the entrance to the final part of the fixed bed reactor.[20] Correspondingly, a gradual decrease of coke deposition along the catalyst bed was also observed with the most coked zone at the entrance, and the portion of the catalyst bed closest to the outlet was still white or light grey with little coke.[194–197] This is attributed to different methanol concentrations along the reactor resulting in different deactivation rates.[70]

The novel techniques have thus provided extensive new evidence for a variety of intermediate molecules in the formation of both products as well as deactivating species in all stages of the process. The role of cage crossing species in the formation of non-dissolvable coke species was demonstrated for CHA-zeolites. Evidence for the proximity of coke clusters and active acid sites was provided, and oriented zeolite films were used to demonstrate that surface plays an important role in the deactivation of ZSM-5 catalysts for MTH.

4.2.3. Propane dehydrogenation Process

Coke deposition in the PDH process is relatively slow, which implies that the early stages of the process can conveniently be monitored using in situ or even operando spectroscopic tools. Over the years, different analytical tools have developed from single probes to combined multi-technique reactor systems that can simultaneously monitor catalyst active sites and coke precursors, summarized in Figure 14.

Sattler et al., for instance, studied the PDH process with a pilot-scale unit with a combined operando UV/Vis and Raman spectroscopy setup, with optical fiber probes at different heights in the reactor bed.[86,200] The development of coke species over time could be differentiated by the intensity ratio between the D1 (disordered edges of graphene layers[201]) and G (ideal graphitic lattice[201]) Raman peaks. On Pt/Sn-based PDH catalyst materials, Wang et al.,[202] using a range of analytical techniques, including HR-TEM, FT-IR, TGA, and pyrolysis GC/MS, report most of the coke is aliphatic, and is at or near the metal particles, but with DRIFT they do observe the conversion of the softer coke to more aromatic coke. Li et al.,[87] using a combination of TGA/TPO, Raman spectroscopy and IR spectroscopy, observe two different coke species, one on the acidic support, and a softer coke, that can be formed without interaction with the acid sites, on the metal particles. Both Li et al. and Wang et al.[87,202] suggest this softer coke is formed through simple propene oligomerization.

Iglesias-Juez et al.[199] studied the deactivation of Pt(Sn) PDH catalyst materials using an in situ system that allowed for combined time-resolved UV-Vis and Raman spectroscopy, and high-energy resolution X-ray absorption spectroscopy under industrial reaction conditions. High-Energy Resolution Fluorescence Detected (HERFD) XANES[199] was used to follow the dynamics of the Pt-Sn interactions and structure-electronic properties in the metal particles, while the combined UV/Vis and Raman spectroscopy were used to monitor the coke formation and activity changes over time (again using the D/G band intensity ratios). The combination of UV/Vis, Raman, and XAFS in one operando reactor system was first described by Beale et al. and Ramaker et al.[203,204] in a system that was used to study Mo-based PDH catalysts.

Pham et al.[198] show that the loss of activity of alumina-supported platinum catalysts for PDH does not necessarily correlate with coke build-up. Aberration-corrected scanning transmission electron microscopy (STEM) experiments seem to indicate that the in Sn-promoted catalyst, the atomically dispersed Sn atoms assist in the redispersion of the sintered Pt metal nanoparticles during oxidative regeneration, whereas in the absence of Sn, this does not happen.

On related γ-alumina supported Pt-Re reforming catalysts, Bare et al.[169] describe a multi-technique approach combining laser Raman, ^{13}C-MAS-NMR, TPO, XPS, and carbon K-edge NEXAFS to study, post-mortem, the various coke species. They conclude the majority of the coke species can be found in contact with the support, and consisting of incomplete medium-sized graphene-like rafts built from smaller polycyclic aromatic species.

The new techniques have thus allowed for the in situ analysis of the coke forming species in the reactor in various stages of deactivation, and allowed for the distinction of coke species at the metal surface and the support surface and their respective role in the deactivation process.

4.2.4. Fischer–Tropsch synthesis process

Since FTS converts C_1-species, namely as CO together with H_2, to long-chain hydrocarbons, fouling by waxy products is a factor in deactivation of the catalysts by carbon deposition. These species could block the pores or prevent access to the metal active sites. Iron-based FTS catalysts and nickel-based catalysts for CO_2 methanation or MSR can deactivate by the formation of carbon filaments that are strong enough to disintegrate catalyst particles and block the reactor pipes. The formation of these filaments can be visualized with TEM.[105,114] During the reaction, the environment contains CO and H_2 (i.e., synthesis gas), various hydrocarbons, and water. The iron-based FTS catalysts thus are thought to be complex mixtures of iron oxide, metal and carbide phases. The analysis of the reaction and the catalyst deactivation by carbon deposition therefore focuses mainly on the iron species.[90] Mössbauer spectroscopy,[205–207] Auger Electron

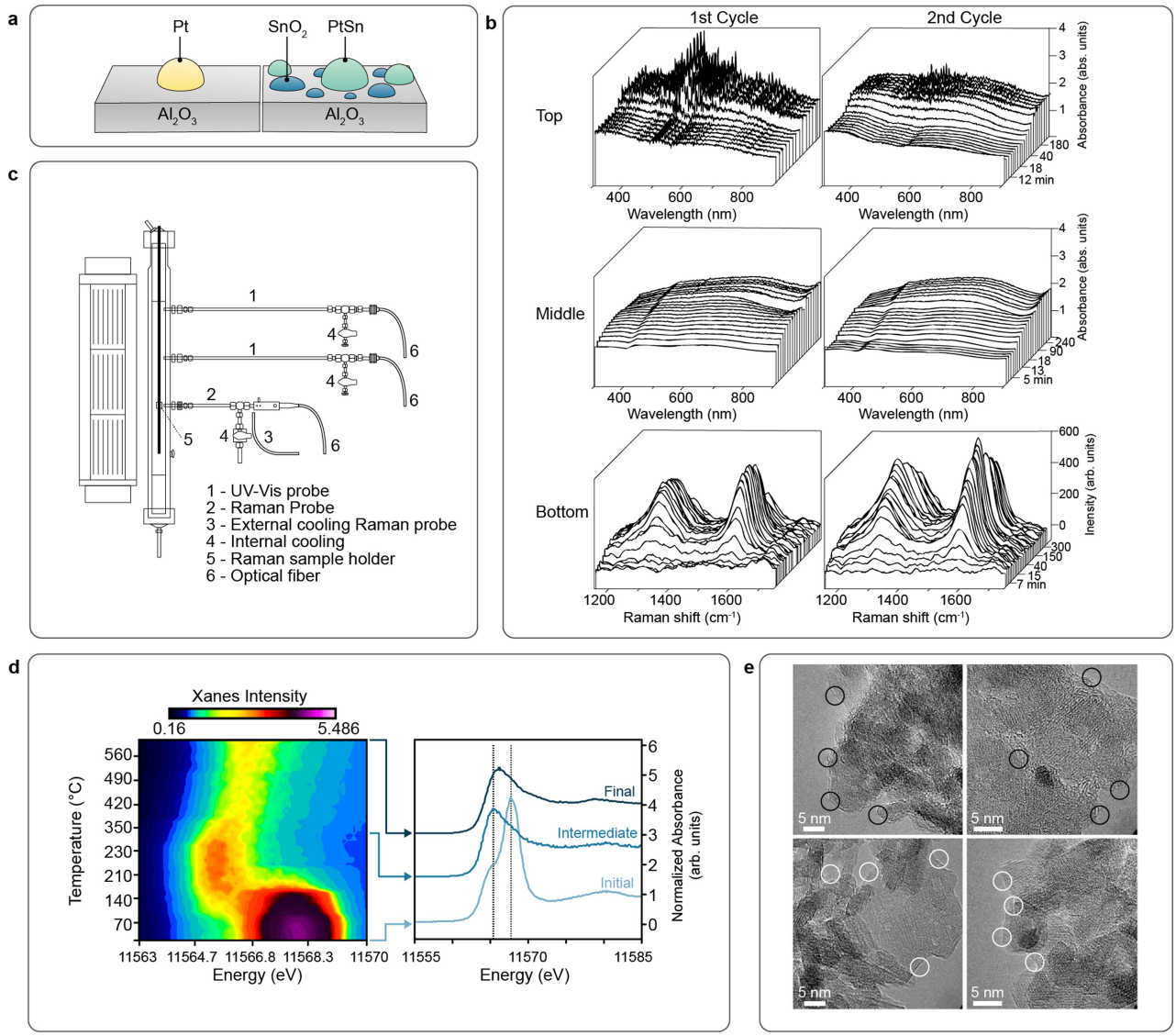

Figure 14. Recent techniques for the study of coke deposits in propane dehydrogenation (PDH) catalysts. Panel A depicts the catalyst, in this case Sn-doped Pt on Al_2O_3 (Reproduced from Pham et al.[198] under the terms and conditions of the Creative Commons CC-BY 4.0 license. Copyright © 2016 American Chemical Society.). Panel B: Operando UV/Vis and Raman spectra as reported by Sattler et al.[86] (see also Panel C) (Reprinted with permission from Wiley. Copyright © 2014 Wiley) Panel C: A reactor design for in situ UV/Vis and Raman spectroscopy was described by Sattler et al.[86] (Reprinted with permission from Wiley. Copyright © 2014 Wiley) Panel D: Iglesias-Juez et al.[199] used high-energy resolution fluorescence detected X-ray absorption near-edge structure (HERFD-XANES) (Reprinted with permission from Elsevier. Copyright © 2010 Elsevier), Panel E: Pham et al.[198] applied transmission electron microscopy (TEM). (Reproduced under the terms and conditions of the Creative Commons CC-BY 4.0 license. Copyright © 2016 American Chemical Society.)

Spectroscopy (AES),[208,209] IR, Raman, UV/Vis, and XRD are commonly used[90] for the analysis of the iron oxides/metal/carbides (see Figure 15). De Smit et al., for instance, describe an integrated in situ XRD/XAFS/Raman setup for studying e-, c-, and θ-Iron carbides in FTS synthesis.[91] In addition, HRTEM-EDX can provide insight in the formation of active species and deactivation routes,[92,93] SEM and TEM in general provide intriguing images of the carbon nanofibers.[105,114]

Moodley et al.[210] have reviewed the deactivation of cobalt-based FTS catalysts. They conclude that is difficult to study the carbon species that cause deactivation, because in essence they are part of the desired reaction product. The polymeric carbon species were observed with energy-filtered TEM (EFTEM) and high-sensitivity low energy ion scattering (HS-LEIS), and were shown to be located both on the support and the supported cobalt metal nanoparticles. The work[210] seems to indicate that the formation of carbides is less important in the deactivation of cobalt based FTS catalysts as compared to iron-based FTS catalysts, as also suggested by Niemantsverdriet and van der Kraan,[211] who indicate that the rate of formation of carbides is much slower for cobalt and nickel compared to iron. In the case of iron, the rate of formation of carbides even appears to be

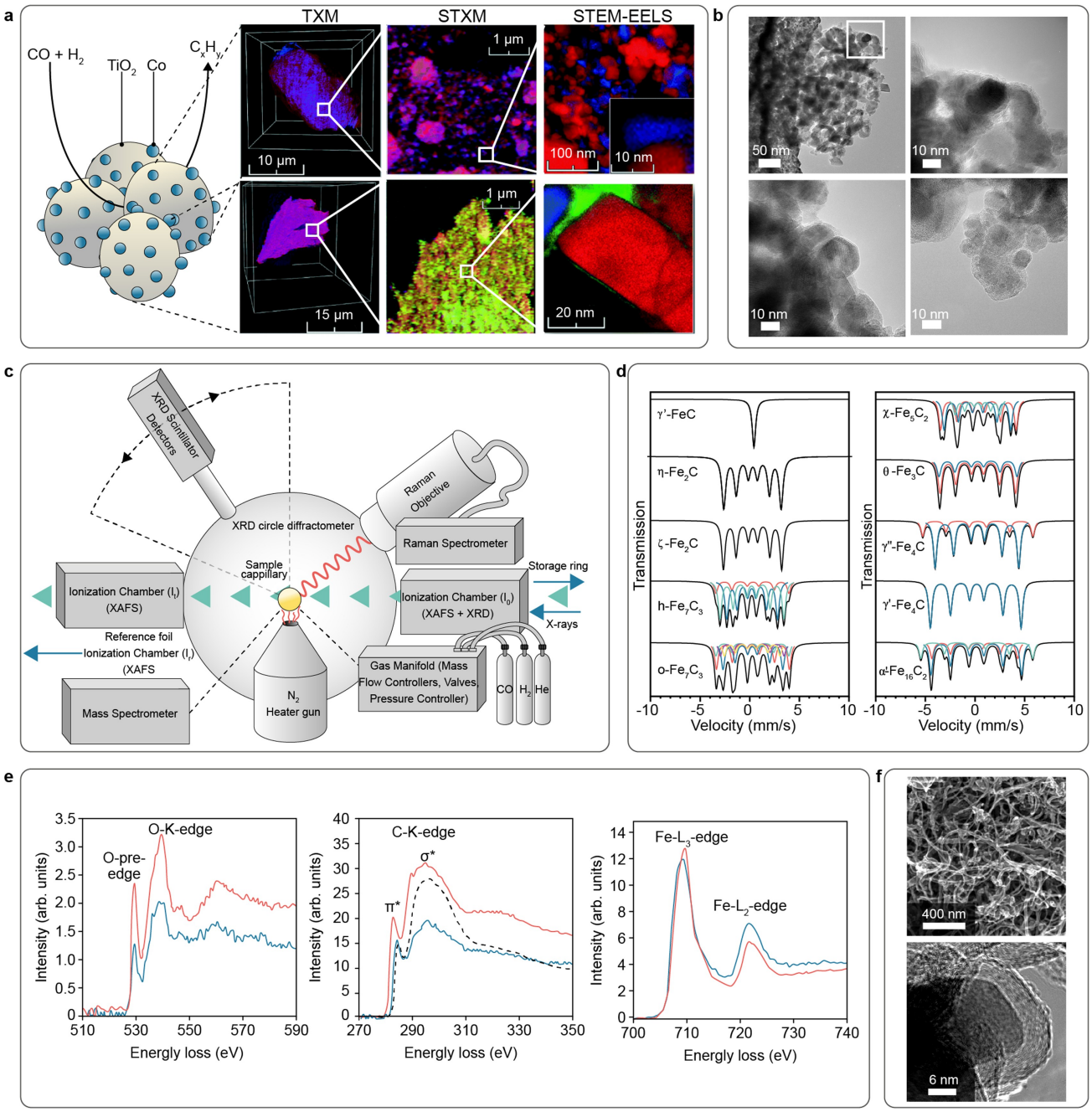

Figure 15. An overview of techniques to study coke formation in Fischer–Tropsch synthesis (FTS) catalysts. Panel A: Cats et al.[140] applied a combination of transmission X-ray microscopy (TXM), scanning transmission X-ray microscopy (STXM) and scanning transmission electron microscopy-electron energy loss spectroscopy (STEM-EELS).(Reproduced with permission from Cats et al.,[140] Copyright © 2016 The Royal Society of Chemistry) Panel B: The transmission electron microscopy (TEM) image shows Fe_xC catalysts (Reprinted from Janbroers et al.[93] with permission from Elsevier. Copyright © 2009 Elsevier). Panel C: de Smit et al.[91] described a system for simultaneous operando Raman spectroscopy, X-ray absorption spectroscopy (XAS) and X-ray diffraction (XRD) (reprinted with permission from the American Chemical Society. Copyright © 2010 American Chemical Society). Panel D: Mössbauer spectroscopy is frequently used to study Fe-compounds (Reproduced from Liu et al.[205] under the terms and conditions of the Creative Commons CC-BY 4.0 license. Copyright © 2016 The Author(s)), Panel E: EELS was used by Janbroers et al.[93] (Reprinted with permission from Elsevier. Copyright © 2009 Elsevier). Panel F: TEM and scanning electron microscopy (SEM) were used to study carbon nanofibers. The TEM image on the bottom shows a metal particle embedded in the tip of a carbon nanofiber (previously unpublished image provided by Prof. J. W. Geus).

higher than the FTS rate.[211] In a later paper, Saib et al.[212] conclude that the sintering of the cobalt particles, carbon deposition, and possibly CO-induced surface reconstruction are the only significant mechanisms for deactivation of Co-based FTS catalysts. Argyle et al.[213] derive a model for deactivation of Co-based FTS catalysts based on parameters

for sintering (fast) and fouling/coke-deposition (slow). Ahn et al.[214] report carbon-deposition on unsupported precipitated and mesoporous Co_3O_4 catalysts. In the bulk Co-based catalyst prepared by precipitation, the authors observe (in TEM) an amorphous carbon layer (from waxy FTS products) deposited on the cobalt, while for the mesoporous material they actually observe the formation of whiskers (i.e., carbon nanofibers), which they attribute to the presence of small crystallites of Co.

Cats et al. have studied cobalt-based FTS catalyst materials using a combination of Transmission X-Ray Microscopy (TXM), Scanning Transmission X-Ray Microscopy (STXM), and STEM-EELS. In contrast to the conventional strong metal support interactions (SMSI) behaviour, in this catalyst material the cobalt redistributes and spreads over the TiO_2 support surface. XPS and STEM-EELS indicate the formation a layer of amorphous and polyaromatics coke species, as well as the formation of surface cobalt carbide (i.e., Co_2C). This carbide phase may be mobile and transport coke-intermediates to the TiO_2 support phase.

The new techniques have mainly been used in FTS to focus on the identity of the various active species of the catalyst and the role of various (surface) carbides. The coke species (amorphous layers or filaments) were mostly directly observed in (high-resolution) TEM.

4.2.5. Catalytic conversion of municipal and agricultural waste

The analysis of carbon species during the conversion of biomass and plastics, illustrated in Figure 16, seems to focus more on the products formed than on catalyst deactivation. Williams, for instance, reviews the formation of hydrogen and carbon nanotubes from plastic waste,[219] and Liu and Yuan describe the same products from cracking model compounds representing waste cooking oil.[220] The carburisation of biomass and plastics, but also of hydrocarbons, such as methane, may be an interesting option to prepare so-called "turquoise" hydrogen without producing CO_2. Ma et al. describe the structural effects of regeneration of coked catalysts used for lignin pyrolysis using NMR and electron microscopy,[221] but do not analyse the coke species themselves. Parvulescu et al.[215] studied catalyst deactivation during etherification of biomass-based polyols with long linear alkenes on large zeolite crystals with the BEA topology using CFM to visualize the coke deposition, and conclude the reaction (and the deactivation) takes place mainly on the outside of the zeolite crystals. Luna-Murillo et al.[218] studied zeolite HZSM-5-based catalyst extrudates with Al_2O_3 binder for catalytic fast pyrolysis (CFP) of biomass. A combination of optical microscopy, CFM, SEM-EDX and NMR was used to study the deactivation of the catalyst bodies. With pine-wood derived biomass, the authors observed thermal coke from large oligomeric species deposits on the external area of the catalyst extrudates, whereas with cellulose-derived material, catalytic coke derived from smaller oxygenates deposited more inside the catalyst extrudates.

Hernando et al.[222] studied modifications on zeolite HZSM-5 accessibility and acidity, and report that the addition of ZrO_2 greatly reduces the unwanted severe cracking and coking reactions in the catalytic pyrolysis of lignocellulose. The coke on the catalyst material was determined with TGA, whereas the local accessibility of the Brønsted acid sites was studied by following the hydrolysis of 4-fluorostyrene in CFM, like previously performed for FCC catalysts by Buurmans et al.[223] Heracleous et al.[217] further studied the ZrO_2-promoted HZSM-5 materials, among others with the CFM technique, and report that poly-aromatic coke rapidly lays down in an egg-shell distribution blocking the strong Brønsted sites, whereas in later stages of catalyst deactivation a softer coke deposits that blocks the zeolite pore system and external surface. Hernández-Giménez et al.[224] studied the ZrO_2-ZSM-5 system in CFP of oak-derived biomass in extrudate-form using a combination of TPO, CFM, and UV/Vis and FT-IR spectroscopy. The authors observed different coke species (i.e., poly-aromatic, pre-graphitic, and smaller polyaromatics) depending on the amount of size of the pores available in the catalysts (zeolite micro-and mesoporosity, binder). Like ZrO_2-promoted ZSM-5, gallium-promoted ZSM-5 is reported to be an efficient catalyst material for furans aromatization[225] and it was found that the gallium helps to decrease Brønsted acidity and introduces Lewis acidity, which limits coke formation. The study by Uslamin et al. focuses on determining the (changes in the) distribution of acid sites by among others staining methods.[225]

Jongerius et al.[216] studied the liquid-phase reforming (LPR) process of lignin model compounds with ethanol as dissolving agent on a Pt/γ-Al_2O_3 catalyst material. The main focus of this research was to study the changes in the support during the LPR process, but coke formation was also observed in TGA. IR spectroscopy analysis of the samples failed to show coke species, possibly because of low loading. Oxygenates in the lignin seem to prevent the formation of a coke-like layer derived from ethanol.

The new techniques have thus mostly been used to study the local effects of coke deposition, and visualize the deposition process by various different coke species, and their effects on the local accessibility of the zeolite active sites.

5. Mitigating the effects of coke deposition

Now that we have described the formation mechanisms of different carbon deposits and recent progress in their analysis, we need to turn our attention to mitigating the effects of the deposits. Various mitigation techniques have been developed to slow down or prevent the deactivation, such as metal traps, increased accessibility of the catalyst matrix,[226–228] or introduction of hierarchical pore systems in zeolites.[229,230] Once a catalyst is deactivated, the user is left with a couple of options, that greatly depend on the catalyst and the process:

1) Discard the deactivated catalyst. This option is not preferred in terms of closing the material cycle, but may

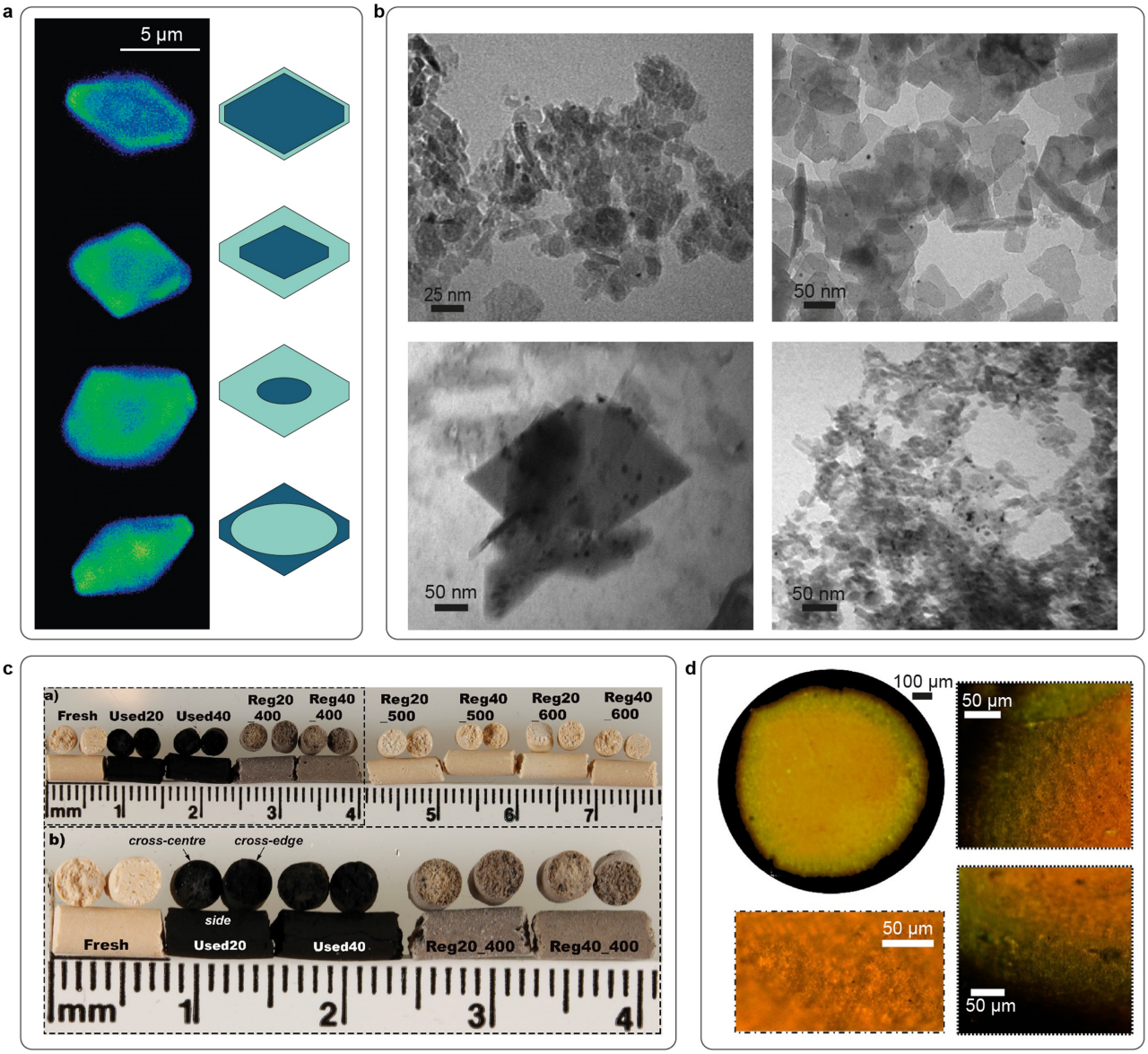

Figure 16. Recent techniques for the study of coke deposits in catalysts used for the conversion of biomass or plastics. Panel A: Parvulescu et al.[215] describe confocal fluorescence microscopy (CFM) on H-BEA zeolite single crystals, (reprinted with permission from the American Chemical Society. Copyright © 2010 American Chemical Society). Panel B: Jongerius et al.[216] applied transmission electron microscopy (TEM) (reprinted with permission from the American Chemical Society. Copyright © 2013 American Chemical Society), Panel C: Heracleous et al.[217] show different degrees of coking by simple visual inspection, Reprinted with permission from Elsevier. Copyright © 2019 Elsevier). Panel D: Luna-Murillo et al.[218] describe CFM images on cross-sections of catalyst extrudates. (Reproduced under the terms and conditions of the Creative Commons CC-BY-NC-ND 4.0 license. Copyright © 2020 American Chemical Society.)

be the most cost-effective solution for low-cost catalysts, like FCC. A small portion of deactivated FCC catalysts is landfilled.

2) Re-use the catalyst in a less demanding operation. There is a sizeable market for example in equilibrium FCC catalysts that are re-used in FCC, among others for unit startup. In addition, deactivated FCC catalysts can be re-used as raw material for building applications.
3) Disassemble the catalyst and reclaim the (precious) metals present in metal-based solid catalysts. This option closes the material cycle and ensures efficient (re-) use of scarce raw materials.
4) Rejuvenate the catalyst to regain essentially fresh activity levels. For simple solid acid catalysts the latter may require controlled burning of the coke, for other types of catalysts more elaborate procedures are required. We will describe the in situ regeneration of FCC catalysts and solid acid alkylation process during the process,[101] and ex situ rejuvenation process commonly applied in HPC.[231] We will differentiate between catalyst regeneration, which happens as part of the regular catalytic process, and catalyst rejuvenation, which involves an ex situ treatment.

5.1. Catalyst and process design

Rapid catalyst deactivation, such as observed in the FCC process,[26,27] calls for *in-process regeneration strategies*: the catalyst cycles between a short stay (seconds) in a cracking zone and longer stay (minutes) in a regeneration zone several times an hour. This removes most of the carbon deposits. A similar approach is observed in solid acid alkylation, in which a multi-reactor system is employed: the process cycles between an active reactor where alkylation takes place and a reactor in regeneration configuration. A third reactor provides the option for more extensive regeneration if needed.

In addition, catalyst manufacturers can tune the *pore system* of the catalyst to allow more easy access of large feedstock reaction molecules to active sites, or more easy egress of trapped product species e.g. during steam stripping.[226] Recent 3D X-ray spectroscopy have allowed the analysis of the actual pore network and the sensitivity of the diffusion process to disturbances by deposition of poisons.[155–157,165] Expanding from FCC to general catalyst design terms, a hierarchical 3D-interconnected pore system, with large pores on the surface, and gradual decreasing pore diameters towards the center of the particle should be less susceptible to pore blockages in general.[182] However, such a hierarchical pore system on catalyst particle scale (50 mm-several mm) is hard to synthesize, and in addition, there is a trade-off between catalyst porosity and particle strength. Hierarchical pore systems on zeolite particle level (nm-mm) are more easily prepared, and have been studied extensively.[230,232,233]

Metal traps can assist in removing species that might develop unwanted catalytic effects, such as nickel and vanadium in FCC catalysts.[25] Nickel (and iron) species deposited from the feedstock may develop into dehydrogenation catalysts that help catalyze coke formation, vanadium may destroy the zeolite. The removal of nickel species in the FCC process is realized by the addition of special components that react with nickel to form harmless species that are hard to reduce to metallic nickel.

Promotors can be added to the catalyst to assist in in-process removal of unwanted species. Franz et al.[234] describe the effect of the addition of small amounts of Na, K, or Cs on ZrO_2-supported catalysts for methane dry reforming. The promotors help block coke-forming site at low loading, and in addition assist in coke-gasification. Alipour et al.[235] describe the promotion of Al_2O_3-supported nickel catalysts for methane steam reforming catalysts with alkaline earth oxides (Mg, Ca, Ba), and report suppressed coke formation. Meima and Menon[236] describe the use of K as a promotor for coke gasification in iron oxide based ethylbenzene dehydrogenation catalysts. In PDH, the addition of tin as a promoter affects the size and geometry of the active particles on Pt/Al_2O_3 catalysts, which improves coke selectivity, among others by changing the adsorption of coke precursors on the active sites, as well as influencing the dehydrogenation reactions. Just like in the other dehydrogenation processes mentioned above, alkali metals such as K also work here, possible by blocking acid sites.[61]

5.2. Catalyst regeneration

Zhou et al.[237] recently reviewed the different strategies for regeneration of deactivated catalyst materials. Common regeneration approaches include oxidation, gasification, and hydrogenation. Catalyst regeneration can be an integral part of the process design, as demonstrated in the FCC process.[25] Rapid coke deposition in the cracking step is followed by controlled burn-off of the coke deposits. Due to diffusion limitations and limited residence time, the oxidation of the coke deposits is not complete, and hard coke deposits remain in the catalyst and build up over time. In solid acid alkylation, the deactivation by softer coke species, longer chain branched alkanes and alkenes occurs over a longer time period. The removal of these softer coke species requires a process step under relatively mild conditions,[101] that can be limited to normal process temperatures if performed before the onset of heavier coke species formation. The removal of olefins from the reactant stream can be sufficient to perform this mild regeneration. Over time, heavier coke species build up, that have to be removed with a mild hydrogenation step.

MTH catalysts can also be reactivated by burning off the coke at elevated temperature.[238] The initial process design was a fixed bed system, more recent process designs involve a fluid bed system with continuous regeneration, which looks very much like the FCC process design.[239] The regeneration procedure leads to considerable damage to the zeolite structure, since most of the coke species to be burnt are inside the zeolite structure, and will lead to high local temperature and steam concentrations. Zhou et al.[240] describe a way to convert inactive hydrocarbon pool molecules to active naphthalenes by employing a steam cracking step in the MTH process.[241]

Finally, regeneration of Pt/Sn PDH catalyst materials leads to loss of dispersion of the supported Pt particles. Sn species, which also have a role in controlling the selectivity of the actual dehydrogenation process, appear to be important in the deactivation process. Pham et al.[198] report that isolated Sn-species on the catalyst support serve as anchoring points for the Pt particles, thus inhibiting the observed metal sintering. Furthermore, also for the Cr-based PDH catalyst materials coke deposits can be removed by a regeneration process where the coke is burned off. Unfortunately, the high catalyst temperatures may lead to solid-state conversion processes in which the surface chromium ions gradually migrate into the alumina support matrix, thereby transforming the support ultimately into a dense $CrAlO_x$ phase, which is not (anymore) active for catalytic propane dehydrogenation.

5.3. Catalyst rejuvenation

Although HPC catalysts can be regenerated by burning off the coke deposits, a more desirable treatment is the rejuvenation, which combines a controlled burn-off of coke species with a redispersion of the active metal components.[231] This prevents the obvious risk of sintering

the active metals during the burn-off, or the formation of inactive species like cobalt aluminate. Using rejuvenation, the activity of the catalyst can be sectored to near-original activity, and catalyst lifetime is expanded considerably. Typically, catalysts can be rejuvenated a couple of times before the activity drops too low. Upon reaching this stage, the active metals in HPC catalysts are usually reclaimed, so in theory the HPC catalyst manufacture and use can be considered circular. In practice, the reclaimed metals are not always re-used in catalyst manufacture, but rather in other processes requiring transition metals, such as steel manufacturing.

6. Concluding Remarks

The formation of carbon deposits, which we often coin as coke, in the catalytic conversion processes of hydrocarbons is thermodynamically favored at reaction conditions of many large-scale industrial processes, even when some of these operate at increased hydrogen partial pressure. The active sites or phases that are responsible for the desired catalytic action of the solid catalyst can and will serve as the sites where coke formation pathways initiate. Propagation of the coke formation pathways then can proceed autocatalytically or through non-catalytic (thermal) routes. This implies that solid catalysts and related processes for hydrocarbon conversion reactions need to be designed to minimize detrimental effects of coke deposition. In a very limited number of cases (e.g., those in which filamentous carbon is formed), the design of the active site can assist. By controlling the active metal particle morphology and the crystal planes exposed, the formation of carbide species and their dissociation to graphenic carbon layer forming the filaments can be avoided to a certain extent, since the catalytic reaction and (changes in) process conditions may alter the morphology of the active metal sites during reaction. In most other cases, process design or pore design are the preferred routes. In solid acid alkylation, permanent deactivation of the catalyst (acid sites) can be avoided by interrupting the process well before irreversible damage has been done, and removing reaction intermediates from the catalyst surface. In FCC, the catalyst is regenerated after each brief cracking step by burning off (most of) the carbon deposits in a longer regenerative step. The effect of deactivation by pore plugging can be mitigated to a certain extent by careful design of the pore system, such as post-synthesis mesopore formation in zeolites. Of course, apart from the effects of pore plugging, catalyst designers also have to take into account mass transfer of reactants and products, as well as macroscopic effects such as strength of the catalyst particles, which may restrict the options.

It is clear that novel analytical tools provide new possibilities for following spatial and temporal development of catalytic coke species under realistic conditions. The resolution of X-ray microscopy and tomography tools is at present limited to the mesopore range (i.e., around 20–50 nanometers at the moment), so the interface of support pores, zeolite mesopores, and zeolite micropores at <10 nanometer still eludes direct observation. Combination of (micro-)spectroscopic techniques, such as confocal fluorescence microscopy and UV/Vis spectroscopy, with well-designed model reaction systems may provide novel information for coking analysis under operando/in situ conditions. The direct observation of low-Z elements, such as carbon at nanometer-resolution, has recently been demonstrated.[155] Computer modeling of pore blockage by coke-forming reactions requires analytical tools and related resources that are as yet not available and may require multi-scale approaches. In spite of the challenges mentioned above, fundamental understanding of the coke formation processes at various length scales will assist in the design of improved catalyst materials, that are ready for the conversion of ever heavier fossil feedstocks. More importantly, better solid catalysts and related chemical conversion processes will allow for more effective use of critical raw materials, and will assist in the transformation of our present fossil-fuel based economy to a carbon-neutral society that will benefit from new routes to platform molecules, new building blocks, and new processes to close the material loops, thereby ultimately create a more sustainable society.

Acknowledgements

BMW acknowledges funding from the Netherlands Research Council (NWO) in the frame of a Gravitation Program (Multiscale Catalytic Energy Conversion, MCEC), the Advanced Research Consortium (ARC) Chemical Building Blocks Consortium (CBBC), as well as the European Research Council (ERC) Advanced Grant (no. 321140) and ERC Proof-of-Concept grant (no. 862283). The authors thank Dr. Thomas Hartman (Utrecht University) for the help with the design of some of the figures.

Conflict of Interest

The authors declare no conflict of interest.

Keywords: Carbon Deposition · Catalyst Deactivation · Catalyst Design · Coke · Coke Analysis

[1] M. Guisnet, F. R. Ribeiro, *Deactivation and Regeneration of Zeolite Catalysts*, Imperial College Press, London, **2011**.
[2] C. Bartholomew, *Kirk-Othmer Encycl. Chem. Technol.*, Wiley, Hoboken, **2003**.
[3] M. D. Argyle, C. H. Bartholomew, *Catalysts* **2015**, *5*, 145–269.
[4] C. H. Bartholomew, *Appl. Catal. A* **2001**, *212*, 17–60.
[5] J. G. Speight, *Korean J. Chem. Eng.* **1998**, *15*, 1–8.
[6] C. H. Bartholomew, *Catal. Rev.* **1982**, *24*, 67–112.
[7] D. Trimm, *Catalysts in Petroleum Refining 1989, Stud. Surf. Sci. Catal., Vol. 53* (Eds.: D. L. Trimm, S. Akashah, M. Absi-Halabi, A. Bishara), Elsevier Science Publishers B. V., Amsterdam, **1989**, pp. 41–60.
[8] D. L. Trimm, *Appl. Catal.* **1983**, *5*, 263–290.
[9] J. Rostrup-Nielsen, D. L. Trimm, *J. Catal.* **1977**, *48*, 155–165.

[10] *Catalyst Deactivation: Proceedings of the International Symposium, Antwerp, October 13–15, 1980, Stud. Surf. Sci. Catal., Vol. 6* (Eds.: B. Delmon, G. F. Froment), Elsevier, Amsterdam, **1980**.

[11] *Catalyst Deactivation: Based on the Invited Contributions to the Third International Symposium on Catalyst Deactivation and Poisoning (ISCDAP 3) Held June 19–21, 1985, at the Lawrence Berkeley Laboratory, Chemical Industries, Vol. 30* (Eds.: E. E. Petersen, A. T. Bell), Dekker, New York, **1987**.

[12] *Catalyst Deactivation 1987: Proceedings of the 4th International Symposium, Antwerp, September 29–October 1, 1987, Stud. Surf. Sci. Catal., Vol. 34* (Eds.: B. Delmon, G. F. Froment), Elsevier, Amsterdam, **1987**.

[13] *Catalyst Deactivation, 1991: Proceedings of the 5th International Symposium, Evanston IL, June 24–26, 1991, Stud. Surf. Sci. Catal., Vol. 68* (Eds.: C. H. Bartholomew, J. B. Butt), Elsevier, Amsterdam, **1991**.

[14] *Catalyst Deactivation, 1994: Proceedings of the 6th International Symposium, Ostend (Belgium), October 3–5, 1994, Stud. Surf. Sci. Catal., Vol. 88* (Eds.: B. Delmon, G. F. Froment), Elsevier, Amsterdam, **1994**.

[15] *Catalyst Deactivation 1997: Proceedings of the International Symposium, Cancun, Mexico, October 5–8, 1997, Stud. Surf. Sci. Catal., Vol. 111* (Eds.: C. H. Bartholomew, G. A. Fuentes), Elsevier, Amsterdam, **1997**.

[16] *Catalyst Deactivation 1999: Proceedings of the 8th International Symposium, Brugge, Belgium, October 10–13, 1999, Stud. Surf. Sci. Catal., Vol. 126* (Eds.: B. Delmon, G. F. Froment), Elsevier, Amsterdam, **1999**.

[17] *Catalyst Deactivation 2001: Proceedings of the 9th International Symposium, Lexington, KY, USA, October 7–10, 2001, Stud. Surf. Sci. Catal., Vol. 139* (Eds.: J. J. Spivey, G. W. Roberts, B. H. Davis), Elsevier, Amsterdam, **2001**.

[18] A. J. Martín, S. Mitchell, C. Mondelli, S. Jaydev, J. Pérez-Ramírez, *Nat. Catal.* **2022**, *5*, 854–866.

[19] H. G. Karge, *Stud. Surf. Sci. Catal., Vol. 137* (Eds.: H. van Bekkum, E. M. Flanigen, P. A. Jacobs, J. C. Jansen), Elsevier, Amsterdam, **2001**, pp. 707–746.

[20] U. Olsbye, S. Svelle, K. P. Lillerud, Z. H. Wei, Y. Y. Chen, J. F. Li, J. G. Wang, W. B. Fan, *Chem. Soc. Rev.* **2015**, *44*, 7155–7176.

[21] H. S. Cerqueira, C. Sievers, G. Joly, P. Magnoux, J. A. Lercher, *Ind. Eng. Chem. Res.* **2005**, *44*, 2069–2077.

[22] J.-O. Barth, A. Jentys, J. A. Lercher, *Ind. Eng. Chem. Res.* **2004**, *43*, 2368–2375.

[23] B. Liu, D. Slocombe, M. AlKinany, H. AlMegren, J. Wang, J. Arden, A. Vai, S. Gonzalez-Cortes, T. Xiao, V. Kuznetsov, P. P. Edwards, *Appl. Petrochem. Res.* **2016**, *6*, 209–215.

[24] S. Ilias, A. Bhan, *ACS Catal.* **2013**, *3*, 18–31.

[25] E. T. C. Vogt, B. M. Weckhuysen, *Chem. Soc. Rev.* **2015**, *44*, 7342–7370.

[26] M. den Hollander, M. Makkee, J. Moulijn, *Stud. Surf. Sci. Catal., Vol. 111* (Eds.: C. H. Bartholomew, G. A.Fuentes), Elsevier, Amsterdam, **1997**, pp. 295–302.

[27] M. den Hollander, M. Makkee, J. Moulijn, *Catal. Today* **1998**, *46*, 27–35.

[28] M. Guisnet, P. Magnoux, *Appl. Catal.* **1989**, *54*, 1–27.

[29] M. Guisnet, P. Magnoux, *Appl. Catal. A* **2001**, *212*, 83–96.

[30] I. Vollmer, M. J. F. Jenks, M. C. P. Roelands, R. J. White, T. van Harmelen, P. de Wild, G. P. van der Laan, F. Meirer, J. T. F. Keurentjes, B. M. Weckhuysen, *Angew. Chem. Int. Ed.* **2020**, *59*, 15402–15423.

[31] I. Vollmer, M. J. F. Jenks, R. Mayorga González, F. Meirer, B. M. Weckhuysen, *Angew. Chem. Int. Ed.* **2021**, *60*, 16101–16108.

[32] S. K. Maity, *Renewable Sustainable Energy Rev.* **2015**, *43*, 1427–1445.

[33] B. Kumar, P. Verma, *Fuel* **2021**, *288*, 119622–119622.

[34] X. Han, H. Wang, Y. Zeng, J. Liu, *Energy Convers. Manag.* **2020**, 100069.

[35] Z. Wang, K. G. Burra, T. Lei, A. K. Gupta, *Prog. Energy Combust. Sci.* **2021**, *84*, 100899.

[36] C. Xu, E. Paone, D. Rodríguez-Padrón, R. Luque, F. Mauriello, *Renewable Sustainable Energy Rev.* **2020**, *127*, 109852.

[37] C. S. Lancefield, B. Fölker, R. C. Cioc, K. Stanciakova, R. E. Bulo, M. Lutz, M. Crockatt, P. C. A. Bruijnincx, *Angew. Chem. Int. Ed.* **2020**, *59*, 23480–23484.

[38] S. Gupta, P. Mondal, V. B. Borugadda, A. K. Dalai, *Environ. Technol. Innov.* **2021**, *21*, 101276.

[39] M. C. Barnés, M. M. de Visser, G. van Rossum, S. R. A. Kersten, J. P. Lange, *J. Anal. Appl. Pyrolysis* **2017**, *125*, 136–143.

[40] B. M. Weckhuysen, D. Wang, M. P. Rosynek, J. H. Lunsford, *J. Catal.* **1998**, *175*, 338–346.

[41] B. M. Weckhuysen, D. Wang, M. P. Rosynek, J. H. Lunsford, *J. Catal.* **1998**, *175*, 347–351.

[42] B. M. Weckhuysen, D. Wang, M. P. Rosynek, J. H. Lunsford, *Angew. Chem. Int. Ed. Engl.* **1997**, *36*, 2374–2376.

[43] C. H. L. Tempelman, E. J. M. Hensen, *Appl. Catal. B* **2015**, *176–177*, 731–739.

[44] B. M. Weckhuysen, M. P. Rosynek, J. H. Lunsford, *Catal. Lett.* **1998**, *52*, 31–36.

[45] N. Kosinov, E. A. Uslamin, L. Meng, A. Parastaev, Y. Liu, E. J. M. Hensen, *Angew. Chem. Int. Ed.* **2019**, *58*, 7068–7072.

[46] I. Yarulina, A. D. Chowdhury, F. Meirer, B. M. Weckhuysen, J. Gascon, *Nat. Catal.* **2018**, *1*, 398–411.

[47] A. D. Chowdhury, K. Houben, G. T. Whiting, M. Mokhtar, A. M. Asiri, S. A. Al-Thabaiti, S. N. Basahel, M. Baldus, B. M. Weckhuysen, *Angew. Chem. Int. Ed.* **2016**, *55*, 15840–15845.

[48] A. D. Chowdhury, A. Lucini Paioni, K. Houben, G. T. Whiting, M. Baldus, B. M. Weckhuysen, *Angew. Chem. Int. Ed.* **2018**, *57*, 8095–8099.

[49] Y. Liu, S. Müller, D. Berger, J. Jelic, K. Reuter, M. Tonigold, M. Sanchez-Sanchez, J. A. Lercher, *Angew. Chem. Int. Ed.* **2016**, *55*, 5723–5726.

[50] T. Sun, W. Chen, S. Xu, A. Zheng, X. Wu, S. Zeng, N. Wang, X. Meng, Y. Wei, Z. Liu, *Chem* **2021**, *7*, 2415–2428.

[51] X. Wu, S. Xu, W. Zhang, J. Huang, J. Li, B. Yu, Y. Wei, Z. Liu, *Angew. Chem. Int. Ed.* **2017**, *56*, 9039–9043.

[52] S. Lee, M. Choi, *J. Catal.* **2019**, *375*, 183–192.

[53] X. Sun, S. Mueller, Y. Liu, H. Shi, G. L. Haller, M. Sanchez-Sanchez, A. C. van Veen, J. A. Lercher, *J. Catal.* **2014**, *317*, 185–197.

[54] S. Müller, Y. Liu, F. M. Kirchberger, M. Tonigold, M. Sanchez-Sanchez, J. A. Lercher, *J. Am. Chem. Soc.* **2016**, *138*, 15994–16003.

[55] J. S. Martinez-Espin, K. de Wispelaere, M. Westgård Erichsen, S. Svelle, T. V. W. Janssens, V. van Speybroeck, P. Beato, U. Olsbye, *J. Catal.* **2017**, *349*, 136–148.

[56] Y. Liu, F. M. Kirchberger, S. Müller, M. Eder, M. Tonigold, M. Sanchez-Sanchez, J. A. Lercher, *Nat. Commun.* **2019**, *10*, 1462.

[57] A. D. Chowdhury, J. Gascon, *Angew. Chem. Int. Ed.* **2018**, *57*, 14982–14985.

[58] P. N. Plessow, F. Studt, *ACS Catal.* **2017**, *7*, 7987–7994.

[59] S. Teketel, M. Westgård Erichsen, F. Lønstad Bleken, S. Svelle, K. Petter Lillerud, U. Olsbye, *Catalysis* (Eds.: J. Spivey, Y.-F. Han, K. Dooley), Royal Society of Chemistry, Cambridge, **2014**, pp. 179–217.

[60] Y. Ono, H. Kitagawa, Y. Sendoda, *J. Chem. Soc. Faraday Trans. 1* **1987**, *83*, 2913–2923.

[61] K. Hemelsoet, V. van Speybroeck, M. Waroquier, *ChemPhysChem* **2008**, *9*, 2349–2358.
[62] V. van Speybroeck, K. Hemelsoet, B. Minner, G. B. Marin, M. Waroquier, *Mol. Simul.* **2007**, *33*, 879–887.
[63] S. Wauters, G. B. Marin, *Chem. Eng. J.* **2001**, *82*, 267–279.
[64] M. Bjørgen, F. Joensen, M. Spangsberg Holm, U. Olsbye, K.-P. Lillerud, S. Svelle, *Appl. Catal. A* **2008**, *345*, 43–50.
[65] P. Sazama, B. Wichterlova, J. Dedecek, Z. Tvaruzkova, Z. Musilova, L. Palumbo, S. Sklenak, O. Gonsiorova, *Microporous Mesoporous Mater.* **2011**, *143*, 87–96.
[66] J. Kim, M. Choi, R. Ryoo, *J. Catal.* **2010**, *269*, 219–228.
[67] M. Choi, K. Na, J. Kim, Y. Sakamoto, O. Terasaki, R. Ryoo, *Nature* **2009**, *461*, 246–249.
[68] D. Rojo-Gama, M. Signorile, F. Bonino, S. Bordiga, U. Olsbye, K. P. Lillerud, P. Beato, S. Svelle, *J. Catal.* **2017**, *351*, 33–48.
[69] M. Bjørgen, S. Svelle, F. Joensen, J. Nerlov, S. Kolboe, F. Bonino, L. Palumbo, S. Bordiga, U. Olsbye, *J. Catal.* **2007**, *249*, 195–207.
[70] S. Müller, Y. Liu, M. Vishnuvarthan, X. Sun, A. C. van Veen, G. L. Haller, M. Sanchez-Sanchez, J. A. Lercher, *J. Catal.* **2015**, *325*, 48–59.
[71] K. Barbera, F. Bonino, S. Bordiga, T. V. W. Janssens, P. Beato, *J. Catal.* **2011**, *280*, 196–205.
[72] B. P. C. Hereijgers, F. Bleken, M. H. Nilsen, S. Svelle, K.-P. Lillerud, M. Bjørgen, B. M. Weckhuysen, U. Olsbye, *J. Catal.* **2009**, *264*, 77–87.
[73] Q. Qian, C. Vogt, M. Mokhtar, A. M. Asiri, S. A. Al-Thabaiti, S. N. Basahel, J. Ruiz-Martínez, B. M. Weckhuysen, *ChemCatChem* **2014**, *6*, 3396–3408.
[74] A. Fonseca, P. Zeuthen, J. B. Nagy, *Fuel* **1996**, *75*, 1413–1423.
[75] S. K. Maity, E. Blanco, J. Ancheyta, F. Alonso, H. Fukuyama, *Fuel* **2012**, *100*, 17–23.
[76] R. Prajapati, K. Kohli, S. K. Maity, M. O. Garg, *Fuel* **2017**, *203*, 514–521.
[77] M. S. Rana, J. Ancheyta, S. K. Sahoo, P. Rayo, *Catal. Today* **2014**, *220–222*, 97–105.
[78] P. Zeuthen, B. H. Cooper, F. T. Clark, D. Arters, *Ind. Eng. Chem. Res.* **1995**, *34*, 755–762.
[79] M. Inoguchi, S. Sakurada, Y. Satomi, K. Inaba, H. Kagaya, K. Tate, T. Mizutori, R. Nishiyama, T. Nagai, S. Onishi, *Bull. Jpn. Pet. Inst.* **1972**, *14*, 153–160.
[80] D. S. Thakur, M. G. Thomas, *Ind. Eng. Chem. Prod. Res. Dev.* **1984**, *23*, 349–360.
[81] S. M. Richardson, H. Nagaishi, M. R. Gray, *Ind. Eng. Chem. Res.* **1996**, *35*, 3940–3950.
[82] K. Fan, X. Yang, J. Liu, L. Rong, *RSC Adv.* **2015**, *5*, 33339–33346.
[83] B. M. Vogelaar, S. Eijsbouts, J. A. Bergwerff, J. J. Heiszwolf, *Catal. Today* **2010**, *154*, 256–263.
[84] B. M. Vogelaar, A. D. van Langeveld, S. Eijsbouts, J. A. Moulijn, *Fuel* **2007**, *86*, 1122–1129.
[85] J. J. H. B. Sattler, A. M. Beale, B. M. Weckhuysen, *Phys. Chem. Chem. Phys.* **2013**, *15*, 12095.
[86] J. J. H. B. Sattler, A. M. Mens, B. M. Weckhuysen, *ChemCatChem* **2014**, *6*, 3139–3145.
[87] Q. Li, Z. Sui, X. Zhou, Y. Zhu, J. Zhou, D. Chen, *Top. Catal.* **2011**, *54*, 888–896.
[88] Z. Lian, C. Si, F. Jan, S. Zhi, B. Li, *ACS Catal.* **2021**, *11*, 9279–9292.
[89] A. Ochoa, J. Bilbao, A. G. Gayubo, P. Castaño, *Renewable Sustainable Energy Rev.* **2020**, *119*, 109600.
[90] E. de Smit, B. M. Weckhuysen, *Chem. Soc. Rev.* **2008**, *37*, 2758–2781.
[91] E. de Smit, F. Cinquini, A. M. Beale, O. V. Safonova, W. van Beek, P. Sautet, B. M. Weckhuysen, *J. Am. Chem. Soc.* **2010**, *132*, 14928–14941.
[92] S. Janbroers, P. A. Crozier, H. W. Zandbergen, P. J. Kooyman, *Appl. Catal. B* **2011**, *102*, 521–527.
[93] S. Janbroers, J. N. Louwen, H. W. Zandbergen, P. J. Kooyman, *J. Catal.* **2009**, *268*, 235–242.
[94] R. T. K. Baker, *Carbon* **1989**, *27*, 315–323.
[95] C. A. Bernardo, J. R. Rostrup-Nielsen, *J. Catal.* **1985**, *96*, 517–534.
[96] J.-W. Snoeck, G. F. Froment, M. Fowles, *Ind. Eng. Chem. Res.* **2002**, *41*, 4252–4265.
[97] E. Rytter, A. Holmen, *Catalysts* **2015**, *5*, 478–499.
[98] J.-F. Xie, Y.-X. Huang, W.-W. Li, X.-N. Song, L. Xiong, H.-Q. Yu, *Electrochim. Acta* **2014**, *139*, 137–144.
[99] C. F. C. Lim, D. A. Harrington, A. T. Marshall, *Electrochim. Acta* **2017**, *238*, 56–63.
[100] H. S. Cerqueira, G. Caeiro, L. Costa, F. Ramôa Ribeiro, *J. Mol. Catal. Chem.* **2008**, *292*, 1–13.
[101] E. T. C. Vogt, G. T. Whiting, A. D. Chowdhury, B. M. Weckhuysen, *Adv. Catal.* **2015**, *58*, 143–314.
[102] C. Liu, R. A. van Santen, A. Poursaeidesfahani, T. J. H. Vlugt, E. A. Pidko, E. J. M. Hensen, *ACS Catal.* **2017**, *7*, 8613–8627.
[103] T. V. W. Janssens, *J. Catal.* **2009**, *264*, 130–137.
[104] T. V. W. Janssens, S. Svelle, U. Olsbye, *J. Catal.* **2013**, *308*, 122–130.
[105] E. T. C. Vogt, A. J. van Dillen, J. W. Geus, *Stud. Surf. Sci. Catal., Vol. 34* (Eds.: B. Delmon, G. F. Froment), Elsevier, Amsterdam, **1987**, pp. 221–233.
[106] P. G. Menon, *J. Mol. Catal.* **1990**, *59*, 207–220.
[107] C. E. Snape, M. C. Diaz, Y. R. Tyagi, S. C. Martin, R. Hughes, *Stud. Surf. Sci. Catal., Vol. 139* (Eds.: J. J. Spivey, G. W. Roberts, B. H. Davis), Elsevier, Amsterdam, **2001**, pp. 359–365.
[108] C. H. Collett, J. McGregor, *Catal. Sci. Technol.* **2016**, *6*, 363–378.
[109] S. van Donk, J. H. Bitter, K. P. de Jong, *Appl. Catal. A* **2001**, *212*, 97–116.
[110] J. F. Haw, D. M. Marcus, in *Handb. Zeolite Sci. Technol.*, Marcel Dekker, New York, **2003**, pp. 1058–1105.
[111] D. Wang, P. Littlewood, T. J. Marks, P. C. Stair, E. Weitz, *ACS Catal.* **2022**, *12*, 8352–8362.
[112] T. E. Detjen, X. Zheng, R. G. Tinger, *In Situ Trim Coke Selectivation of Toluene Disproportionation Catalyst*, WO 2014/200262, **2014**.
[113] A. R. Pradhan, T. S. Lin, W. H. Chen, S. J. Jong, J. F. Wu, K. J. Chao, S. Bin Liu, *J. Catal.* **1999**, *184*, 29–38.
[114] K. P. de Jong, J. W. Geus, *Catal. Rev. Sci. Eng.* **2000**, *42*, 481–510.
[115] K. Y. Mudi, A. S. Abdulkareem, O. S. Azeez, A. S. Kovo, J. O. Tijani, E. J. Eterigho, *Carbon Lett.* **2019**, *29*, 233–253.
[116] D. Chen, H. P. Rebo, K. Moljord, A. Holmen, *Ind. Eng. Chem. Res.* **1997**, *36*, 3473–3479.
[117] U. Olsbye, S. Svelle, M. Bjørgen, P. Beato, T. V. W. Janssens, F. Joensen, S. Bordiga, K. P. Lillerud, *Angew. Chem. Int. Ed.* **2012**, *51*, 5810–5831.
[118] W. Song, H. Fu, J. F. Haw, *J. Am. Chem. Soc.* **2001**, *123*, 4749–4754.
[119] D. Chen, K. Moljord, T. Fuglerud, A. Holmen, *Microporous Mesoporous Mater.* **1999**, *29*, 191–203.
[120] S. Teketel, W. Skistad, S. Benard, U. Olsbye, K. P. Lillerud, P. Beato, S. Svelle, *ACS Catal.* **2012**, *2*, 26–37.
[121] J. J. Spivey, G. W. Roberts, C. A. Querini, in *Catalysis, Vol. 17*, RSC Publishing, Cambridge, **2004**, pp. 166–209.
[122] N. Wang, W. Sun, Y. Hou, B. Ge, L. Hu, J. Nie, W. Qian, F. Wei, *J. Catal.* **2018**, *360*, 89–96.
[123] Q. Qian, J. Ruiz-Martínez, M. Mokhtar, A. M. Asiri, S. A. Al-Thabaiti, S. N. Basahel, B. M. Weckhuysen, *Catal. Today* **2014**, *226*, 14–24.

[124] Q. Qian, J. Ruiz-Martínez, M. Mokhtar, A. M. Asiri, S. A. Al-Thabaiti, S. N. Basahel, H. E. van der Bij, J. Kornatowski, B. M. Weckhuysen, *Chem. Eur. J.* **2013**, *19*, 11204–11215.

[125] I. L. Buurmans, B. M. Weckhuysen, *Nat. Chem.* **2012**, *4*, 873–86.

[126] Y. Liu, F. Meirer, C. M. Krest, S. Webb, B. M. Weckhuysen, *Nat. Commun.* **2016**, *7*, 12634.

[127] M. Guisnet, P. Magnoux, D. Martin, *Stud. Surf. Sci. Catal., Vol. 111* (Eds.: C. H. Bartholomew, G. A. Fuentes), Elsevier, Amsterdam, **1997**, pp. 1–19.

[128] A. Fonseca, P. Zeuthen, J. B. Nagy, *Fuel* **1995**, *74*, 1267–1276.

[129] A. Fonseca, P. Zeuthen, J. B. Nagy, *Fuel* **1996**, *75*, 1363–1376.

[130] O. Bayraktar, E. L. Kugler, *Appl. Catal. A* **2002**, *233*, 197–213.

[131] D. Mance, J. van der Zwan, M. E. Z. Velthoen, F. Meirer, B. M. Weckhuysen, M. Baldus, E. T. C. Vogt, *Chem. Commun.* **2017**, *53*, 3933–3936.

[132] K. Qian, D. C. Tomczak, E. F. Rakiewicz, R. H. Harding, G. Yaluris, W. Cheng, X. Zhao, A. W. Peters, W. R. G. Co, G. Drive, G. Davison, *Energy Fuels* **1997**, *11*, 596–601.

[133] C. E. Snape, B. J. McGhee, J. M. Andresen, R. Hughes, C. L. Koon, G. Hutchings, *Appl. Catal. A* **1995**, *129*, 125–132.

[134] D. Mores, J. Kornatowski, U. Olsbye, B. M. Weckhuysen, *Chem. Eur. J.* **2011**, *17*, 2874–2884.

[135] D. Mores, E. Stavitski, M. H. F. Kox, J. Kornatowski, U. Olsbye, B. M. Weckhuysen, *Chem. Eur. J.* **2008**, *14*, 11320–11327.

[136] H. Shimada, M. Imamura, N. Matsubayashi, T. Saito, T. Tanaka, *Top. Catal.* **2000**, *10*, 265–271.

[137] M. A. Smith, R. F. Lobo, *Microporous Mesoporous Mater.* **2006**, *92*, 81–93.

[138] S. M. Davis, Y. Zhou, M. A. Freeman, D. A. Fischer, G. M. Meitzner, J. L. Gland, *J. Catal.* **1993**, *139*, 322–325.

[139] P. Gallezot, C. Leclercq, J. Barbier, P. Marecot, *J. Catal.* **1989**, *116*, 164–170.

[140] K. H. Cats, J. C. Andrews, O. Stéphan, K. March, C. Karunakaran, F. Meirer, F. M. F. de Groot, B. M. Weckhuysen, *Catal. Sci. Technol.* **2016**, *6*, 4438–4449.

[141] N.-K. Bär, F. Bauer, D. M. Ruthven, B. J. Balcom, *J. Catal.* **2002**, *208*, 224–228.

[142] B. G. Anderson, R. A. van Santen, L. J. van IJzendoorn, *Appl. Catal. A* **1997**, *160*, 125–138.

[143] N. Wang, L. Wang, Y. Zhi, J. Han, C. Zhang, X. Wu, J. Zhang, L. Wang, B. Fan, S. Xu, Y. Zheng, S. Lin, R. Wu, Y. Wei, Z. Liu, *J. Energy Chem.* **2023**, *76*, 105–116.

[144] J. E. Schmidt, J. D. Poplawsky, B. Mazumder, Ö. Attila, D. Fu, D. A. M. de Winter, F. Meirer, S. R. Bare, B. M. Weckhuysen, *Angew. Chem. Int. Ed.* **2016**, *55*, 11173–11177.

[145] L. R. Aramburo, S. Teketel, S. Svelle, S. R. Bare, B. Arstad, H. W. Zandbergen, U. Olsbye, F. M. F. de Groot, B. M. Weckhuysen, *J. Catal.* **2013**, *307*, 185–193.

[146] L. R. Aramburo, J. Ruiz-Martínez, L. Sommer, B. Arstad, R. Buitrago-Sierra, A. Sepúlveda-Escribano, H. W. Zandbergen, U. Olsbye, F. M. F. de Groot, B. M. Weckhuysen, *ChemCatChem* **2013**, *5*, 1386–1394.

[147] U. El-Nafaty, R. Mann, *Chem. Eng. Sci.* **2001**, *56*, 865–872.

[148] P. Gallezot, C. Leclercq, M. Guisnet, P. Magnoux, *J. Catal.* **1988**, *114*, 100–111.

[149] S. van Donk, F. M. F. de Groot, O. Stéphan, J. H. Bitter, K. P. de Jong, *Chem. Eur. J.* **2003**, *9*, 3106–3111.

[150] B. Schuler, G. Meyer, D. Peña, O. C. Mullins, L. Gross, *J. Am. Chem. Soc.* **2015**, *137*, 9870–9876.

[151] J.-O. Barth, A. Jentys, J. A. Lercher, *Ind. Eng. Chem. Res.* **2004**, *43*, 3097–3104.

[152] D. Fu, K. Park, G. Delen, Ö. Attila, F. Meirer, D. Nowak, S. Park, J. E. Schmidt, B. M. Weckhuysen, *Chem. Commun.* **2017**, *53*, 13012–13014.

[153] I. Lezcano-Gonzalez, E. Campbell, A. E. J. Hoffman, M. Bocus, I. V. Sazanovich, M. Towrie, M. Agote-Aran, E. K. Gibson, A. Greenaway, K. de Wispelaere, V. van Speybroeck, A. M. Beale, *Nat. Mater.* **2020**, *19*, 1081–1087.

[154] G. Greetham, "Kerr-gated Raman Spectroscopy," website: https://www.clf.stfc.ac.uk/Pages/Kerr-Gated-Raman-Spectroscopy.aspx, accessed March 23, 2023.

[155] M. Veselý, R. Valadian, L. Merten Lohse, M. Toepperwien, K. Spiers, J. Garrevoet, E. T. C. Vogt, T. Salditt, B. M. Weckhuysen, F. Meirer, *ChemCatChem* **2021**, *13*, 2494–2507.

[156] F. Meirer, S. Kalirai, D. Morris, S. Soparawalla, Y. Liu, G. Mesu, J. C. Andrews, B. M. Weckhuysen, *Sci. Adv.* **2015**, *1*, e1400199.

[157] F. C. Hendriks, F. Meirer, A. V. Kubarev, Z. Ristanović, M. B. J. Roeffaers, E. T. C. Vogt, P. C. A. Bruijnincx, B. M. Weckhuysen, *J. Am. Chem. Soc.* **2017**, *139*, 13632–13635.

[158] M. J. Wulfers, G. Tzolova-Müller, J. I. Villegas, D. Y. Murzin, F. C. Jentoft, *J. Catal.* **2012**, *296*, 132–142.

[159] X. Huang, X. Jiao, M. Lin, K. Wang, L. Jia, B. Hou, D. Li, *Catal. Sci. Technol.* **2018**, *8*, 5740–5749.

[160] H. An, F. Zhang, Z. Guan, X. Liu, F. Fan, C. Li, *ACS Catal.* **2018**, *8*, 9207–9215.

[161] T. Bauer, S. Maisel, D. Blaumeiser, J. Vecchietti, N. Taccardi, P. Wasserscheid, A. Bonivardi, A. Görling, J. Libuda, *ACS Catal.* **2019**, *9*, 2842–2853.

[162] C. Vogt, B. M. Weckhuysen, J. Ruiz-Martínez, *ChemCatChem* **2017**, *9*, 183–194.

[163] J. Goetze, B. M. Weckhuysen, *Catal. Sci. Technol.* **2018**, *8*, 1632–1644.

[164] A. M. Wise, J. N. Weker, S. Kalirai, M. Farmand, D. A. Shapiro, F. Meirer, B. M. Weckhuysen, *ACS Catal.* **2016**, *6*, 2178–2181.

[165] S. Kalirai, U. Boesenberg, G. Falkenberg, F. Meirer, B. Weckhuysen, *ChemCatChem* **2015**, *7*, 3674–3682.

[166] S. R. Bare, M. E. Charochak, S. D. Kelly, B. Lai, J. Wang, Y. K. Chen-Wiegart, *ChemCatChem* **2014**, *6*, 1427–1437.

[167] I. L. C. Buurmans, J. Ruiz-Martínez, W. V. Knowles, D. van der Beek, J. A. Bergwerff, E. T. C. Vogt, B. M. Weckhuysen, *Nat. Chem.* **2011**, *3*, 862–867.

[168] F. C. Hendriks, S. Mohammadian, Z. Ristanović, S. Kalirai, F. Meirer, E. T. C. Vogt, P. C. A. Bruijnincx, H. C. Gerritsen, B. M. Weckhuysen, *Angew. Chem. Int. Ed.* **2018**, *57*, 257–261.

[169] S. R. Bare, F. D. Vila, M. E. Charochak, S. Prabhakar, W. J. Bradley, C. Jaye, D. A. Fischer, S. T. Hayashi, S. A. Bradley, J. J. Rehr, *ACS Catal.* **2017**, *7*, 1452–1461.

[170] F. Meirer, D. T. Morris, S. Kalirai, Y. Liu, J. C. Andrews, B. M. Weckhuysen, *J. Am. Chem. Soc.* **2015**, *137*, 102–105.

[171] D. A. M. de Winter, F. Meirer, B. M. Weckhuysen, *ACS Catal.* **2016**, *6*, 3158–3167.

[172] J. Ihli, D. Ferreira Sanchez, R. R. Jacob, V. Cuartero, O. Mathon, F. Krumeich, C. Borca, T. Huthwelker, W. C. Cheng, Y. Y. Shu, S. Pascarelli, D. Grolimund, A. Menzel, J. A. van Bokhoven, *Angew. Chem. Int. Ed.* **2017**, *56*, 14031–14035.

[173] M. A. Alabdullah, T. Shoinkhorova, A. Dikhtiarenko, S. Ould-Chikh, A. Rodriguez-Gomez, S. Chung, A. O. Alahmadi, I. Hita, S. Pairis, J. Hazemann, P. Castaño, J. Ruiz-Martinez, I. Morales Osorio, K. Almajnouni, W. Xu, J. Gascon, *Catal. Sci. Technol.* **2022**, *12*, 5657–5670.

[174] H. Oji, R. Mitsumoto, E. Ito, H. Ishii, Y. Ouchi, K. Seki, T. Yokoyama, T. Ohta, N. Kosugi, *J. Chem. Phys.* **1998**, *109*, 10409–10418.

[175] J. P. Hofmann, D. Mores, L. R. Aramburo, S. Teketel, M. Rohnke, J. Janek, U. Olsbye, B. M. Weckhuysen, *Chem. Eur. J.* **2013**, *19*, 8533–8542.

[176] Y. Wei, J. Li, C. Yuan, S. Xu, Y. Zhou, J. Chen, Q. Wang, Q. Zhang, Z. Liu, *Chem. Commun.* **2012**, *48*, 3082.

[177] N. Wang, Y. Zhi, Y. Wei, W. Zhang, Z. Liu, J. Huang, T. Sun, S. Xu, S. Lin, Y. He, A. Zheng, Z. Liu, *Nat. Commun.* **2020**, *11*, 1079.
[178] C. Sprung, B. M. Weckhuysen, *J. Am. Chem. Soc.* **2015**, *137*, 1916–1928.
[179] C. Sprung, B. M. Weckhuysen, *Chem. Eur. J.* **2014**, *20*, 3667–3677.
[180] J. E. Schmidt, L. Peng, J. D. Poplawsky, B. M. Weckhuysen, *Angew. Chem. Int. Ed.* **2018**, *57*, 10422–10435.
[181] D. Fu, O. Heijden, K. Stanciakova, J. E. Schmidt, B. M. Weckhuysen, *Angew. Chem. Int. Ed.* **2020**, *59*, 15502–15506.
[182] G. T. Whiting, N. Nikolopoulos, I. Nikolopoulos, A. D. Chowdhury, B. M. Weckhuysen, *Nat. Chem.* **2019**, *11*, 23–31.
[183] D. Rojo-Gama, M. Nielsen, D. Wragg, M. Dyballa, J. Holzinger, H. Falsig, L. F. Lundegaard, P. Beato, R. Y. Brogaard, K. P. Lillerud, U. Olsbye, S. Svelle, *ACS Catal.* **2017**, *12*, 8235–8246.
[184] J. Goetze, I. Yarulina, J. Gascon, F. Kapteijn, B. M. Weckhuysen, *ACS Catal.* **2018**, *8*, 2060–2070.
[185] J. E. Schmidt, L. Peng, A. L. Paioni, H. L. Ehren, W. Guo, B. Mazumder, D. A. M. de Winter, Ö. Attila, D. Fu, A. D. Chowdhury, K. Houben, M. Baldus, J. D. Poplawsky, B. M. Weckhuysen, *J. Am. Chem. Soc.* **2018**, *140*, 9154–9158.
[186] D. E. Perea, I. Arslan, J. Liu, Z. Ristanović, L. Kovarik, B. W. Arey, J. A. Lercher, S. R. Bare, B. M. Weckhuysen, *Nat. Commun.* **2015**, *6*, 7589.
[187] A. Devaraj, M. Vijayakumar, J. Bao, M. F. Guo, M. A. Derewinski, Z. Xu, M. J. Gray, S. Prodinger, K. K. Ramasamy, *Sci. Rep.* **2016**, *6*, 37586.
[188] S. H. van Vreeswijk, M. Monai, R. Oord, J. E. Schmidt, E. T. C. Vogt, J. D. Poplawsky, B. M. Weckhuysen, *Catal. Sci. Technol.* **2022**, *12*, 1220–1228.
[189] D. Fu, J. E. Schmidt, Z. Ristanović, A. D. Chowdhury, F. Meirer, B. M. Weckhuysen, *Angew. Chem. Int. Ed.* **2017**, *56*, 11217–11221.
[190] D. Fu, A. L. Paioni, C. Lian, O. van der Heijden, M. Baldus, B. M. Weckhuysen, *Angew. Chem. Int. Ed.* **2020**, *59*, 20024–20030.
[191] D. S. Wragg, R. E. Johnsen, M. Balasundaram, P. Norby, H. Fjellvåg, A. Grønvold, T. Fuglerud, J. Hafizovic, Ø. B. Vistad, D. Akporiaye, *J. Catal.* **2009**, *268*, 290–296.
[192] D. S. Wragg, R. E. Johnsen, P. Norby, H. Fjellvåg, *Microporous Mesoporous Mater.* **2010**, *134*, 210–215.
[193] F. L. Bleken, K. Barbera, F. Bonino, U. Olsbye, K. P. Lillerud, S. Bordiga, P. Beato, T. V. W. Janssens, S. Svelle, *J. Catal.* **2013**, *307*, 62–73.
[194] F. L. Bleken, T. V. W. Janssens, S. Svelle, U. Olsbye, *Microporous Mesoporous Mater.* **2012**, *164*, 190–198.
[195] J. F. Haw, D. M. Marcus, *Top. Catal.* **2005**, *34*, 41–48.
[196] M. Kaarsholm, F. Joensen, J. Nerlov, R. Cenni, J. Chaouki, G. S. Patience, *Chem. Eng. Sci.* **2007**, *62*, 5527–5532.
[197] D. S. Wragg, M. G. O'Brien, F. L. Bleken, M. Di Michiel, U. Olsbye, H. Fjellvåg, *Angew. Chem. Int. Ed.* **2012**, *51*, 7956–7959.
[198] H. N. Pham, J. J. H. B. Sattler, B. M. Weckhuysen, A. K. Datye, *ACS Catal.* **2016**, *6*, 2257–2264.
[199] A. Iglesias-Juez, A. M. Beale, K. Maaijen, T. C. Weng, P. Glatzel, B. M. Weckhuysen, *J. Catal.* **2010**, *276*, 268–279.
[200] J. J. H. B. Sattler, I. D. González-Jiménez, A. M. Mens, M. Arias, T. Visser, B. M. Weckhuysen, *Chem. Commun.* **2013**, *49*, 1518–1520.
[201] A. Sadezky, H. Muckenhuber, H. Grothe, R. Niessner, U. Pöschl, *Carbon* **2005**, *43*, 1731–1742.
[202] H. Z. Wang, L. L. Sun, Z. J. Sui, Y. A. Zhu, G. H. Ye, D. Chen, X. G. Zhou, W. K. Yuan, *Ind. Eng. Chem. Res.* **2018**, *57*, 8647–8654.
[203] A. M. Beale, A. M. J. van der Eerden, K. Kervinen, M. A. Newton, B. M. Weckhuysen, *Chem. Commun.* **2005**, 3015.
[204] D. Ramaker, D. Gatewood, A. M. Beale, B. M. Weckhuysen, in *AIP Conf. Proc.*, AIP, Stanford, California (USA), **2007**, pp. 619–621.
[205] X.-W. Liu, S. Zhao, Y. Meng, Q. Peng, A. K. Dearden, C.-F. Huo, Y. Yang, Y.-W. Li, X.-D. Wen, *Sci. Rep.* **2016**, *6*, 26184.
[206] J. W. Niemantsverdriet, C. F. J. Flipse, A. M. van der Kraan, J. J. van Loef, *Appl. Surf. Sci.* **1982**, *10*, 302–313.
[207] A. M. van der Kraan, *Hyperfine Interact.* **1988**, *40*, 211–222.
[208] A. G. Sault, *J. Catal.* **1993**, *140*, 121–135.
[209] A. G. Sault, A. K. Datye, *J. Catal.* **1993**, *140*, 136–149.
[210] D. J. Moodley, J. van de Loosdrecht, A. M. Saib, M. J. Overett, A. K. Datye, J. W. Niemantsverdriet, *Appl. Catal. A* **2009**, *354*, 102–110.
[211] J. Niemantsverdriet, A. M. van der Kraan, *J. Catal.* **1981**, *72*, 385–388.
[212] A. M. Saib, D. J. Moodley, I. M. Ciobîcă, M. M. Hauman, B. H. Sigwebela, C. J. Weststrate, J. W. Niemantsverdriet, J. van de Loosdrecht, *Catal. Today* **2010**, *154*, 271–282.
[213] M. D. Argyle, T. S. Frost, C. H. Bartholomew, *Top. Catal.* **2014**, *57*, 415–429.
[214] C.-I. Ahn, H. M. Koo, M. Jin, J. M. Kim, T. Kim, Y.-W. Suh, K. J. Yoon, J. W. Bae, *Microporous Mesoporous Mater.* **2014**, *188*, 196–202.
[215] A. N. Parvulescu, D. Mores, E. Stavitski, C. M. Teodorescu, P. C. A. Bruijnincx, R. J. M. K. Gebbink, B. M. Weckhuysen, *J. Am. Chem. Soc.* **2010**, *132*, 10429–10439.
[216] A. L. Jongerius, J. R. Copeland, G. S. Foo, J. P. Hofmann, P. C. A. Bruijnincx, C. Sievers, B. M. Weckhuysen, *ACS Catal.* **2013**, *3*, 464–473.
[217] E. Heracleous, E. Pachatouridou, A. M. Hernández-Giménez, H. Hernando, T. Fakin, A. L. Paioni, M. Baldus, D. P. Serrano, P. C. A. Bruijnincx, B. M. Weckhuysen, A. A. Lappas, *J. Catal.* **2019**, *380*, 108–122.
[218] B. Luna-Murillo, M. Pala, A. L. Paioni, M. Baldus, F. Ronsse, W. Prins, P. C. A. Bruijnincx, B. M. Weckhuysen, *ACS Sustainable Chem. Eng.* **2021**, *9*, 291–304.
[219] P. T. Williams, *Waste Biomass Valorization* **2021**, *12*, 1–28.
[220] W. Liu, H. Yuan, *Int. J. Energy Res.* **2020**, *44*, 11564–11582.
[221] Z. Ma, A. Ghosh, N. Asthana, J. van Bokhoven, *ChemCatChem* **2018**, *10*, 4431–4437.
[222] H. Hernando, A. M. Hernández-Giménez, C. Ochoa-Hernández, P. C. A. Bruijnincx, K. Houben, M. Baldus, P. Pizarro, J. M. Coronado, J. Fermoso, J. Čejka, B. M. Weckhuysen, D. P. Serrano, *Green Chem.* **2018**, *20*, 3499–3511.
[223] I. L. C. Buurmans, E. A. Pidko, J. M. de Groot, E. Stavitski, R. A. van Santen, B. M. Weckhuysen, *Phys. Chem. Chem. Phys.* **2010**, *12*, 7032–40.
[224] A. M. Hernández-Giménez, E. Heracleous, E. Pachatouridou, A. Horvat, H. Hernando, D. P. Serrano, A. A. Lappas, P. C. A. Bruijnincx, B. M. Weckhuysen, *ChemCatChem* **2021**, *13*, 1207–1219.
[225] E. A. Uslamin, B. Luna-Murillo, N. Kosinov, P. C. A. Bruijnincx, E. A. Pidko, B. M. Weckhuysen, E. J. M. Hensen, *Chem. Eng. Sci.* **2019**, *198*, 305–316.
[226] A. C. Psarras, E. F. Iliopoulou, L. Nalbandian, A. A. Lappas, C. Pouwels, *Catal. Today* **2007**, *127*, 44–53.
[227] M. Falco, E. Morgado, N. Amadeo, U. Sedran, *Appl. Catal. A* **2006**, *315*, 29–34.
[228] U. El-Nafaty, R. Mann, *Chem. Eng. Sci.* **1999**, *54*, 3475–3484.
[229] J. García-Martínez, M. Johnson, J. Valla, K. Li, J. Y. Ying, *Catal. Sci. Technol.* **2012**, *2*, 987.
[230] K. Li, J. Valla, J. Garcia-Martinez, *ChemCatChem* **2014**, *6*, 46–66.

[231] P. Laveille, A. H. Chaudhry, A. Riva, A. Salameh, G. Singaravel, P. Dufresne, S. Morin, M. Berthod, *Oil Gas Sci. Technol.* **2018**, *73*, 59.
[232] J. Groen, J. Moulijn, J. Pérez-Ramírez, *Ind. Eng. Chem.* **2007**, *46*, 4193–4201.
[233] D. Verboekend, J. Pérez-Ramírez, *ChemSusChem* **2014**, *7*, 753–764.
[234] R. Franz, T. Kühlewind, G. Shterk, E. Abou-Hamad, A. Parastaev, E. Uslamin, E. J. M. Hensen, F. Kapteijn, J. Gascon, E. A. Pidko, *Catal. Sci. Technol.* **2020**, *10*, 3965–3974.
[235] Z. Alipour, M. Rezaei, F. Meshkani, *J. Ind. Eng. Chem.* **2014**, *20*, 2858–2863.
[236] G. R. Meima, P. G. Menon, *Appl. Catal. A* **2001**, *212*, 239–245.
[237] J. Zhou, J. Zhao, J. Zhang, T. Zhang, M. Ye, Z. Liu, *Chin. J. Catal.* **2020**, *41*, 1048–1061.
[238] F. Schmidt, C. Hoffmann, F. Giordanino, S. Bordiga, P. Simon, W. Carrillo-Cabrera, S. Kaskel, *J. Catal.* **2013**, *307*, 238–245.
[239] F. J. Keil, *Microporous Mesoporous Mater.* **1999**, *29*, 49–66.
[240] J. Zhou, M. Gao, J. Zhang, W. Liu, T. Zhang, H. Li, Z. Xu, M. Ye, Z. Liu, *Nat. Commun.* **2021**, *12*, 17.
[241] S. H. van Vreeswijk, B. M. Weckhuysen, *Joule* **2021**, *5*, 757–759.

Manuscript received: January 7, 2023
Accepted manuscript online: April 13, 2023
Version of record online: May 3, 2023